Resilient Vertical Forest Renovation of Reinforced Concrete Structures in Seismic Prone Areas

(H.F.R.I. Project Number 015376)

Investigation of the scenario of high –rise renovated VF building subjected to multiple earthquakes and real time health monitoring

Deliverable D4.1 Work package 4

Funding source

“Hellenic Foundation for Research & Innovation (H.F.R.I.)
Greece 2.0
Basic Research Financing Action”

Host Organization

Democritus University of Thrace (DUTH)

Collaborating Organizations

Aristotle University of Thessaloniki (AUTH)

December 2025

Funded by the European Union
NextGenerationEU

The research project is implemented in the framework of H.F.R.I call “Basic research Financing (Horizontal support of all Sciences)” under the National Recovery and Resilience Plan “Greece 2.0” funded by the European Union – NextGenerationEU (H.F.R.I. Project Number: 015376)

Version	Date	Comments-Modifications
1	December 2025	Final Version
2		

Suggested citation:

Rousakis T., Vanian V., Fanaradelli T., Voutetaki M., Zapris A., Theodoridou I., 2025. Investigation of the scenario of high–rise renovated VF building subjected to multiple earthquakes and real time health monitoring. Greenergy-Resilient Vertical Forest Renovation of Reinforced Concrete Structures in Seismic Prone Areas (H.F.R.I. Project Number 015376). Deliverable D4.1 Democritus University of Thrace, Xanthi.

Project Title	Resilient Vertical Forest Renovation of Reinforced Concrete Structures in Seismic Prone Areas
Acronym	GREENERGY
HFRI Project Number	015376
Call identifier	Basic Research Financing (Horizontal support for all Sciences), National Recovery and Resilience Plan (Greece 2.0) / Sub-action 2. Funding Projects in Leading-Edge Sectors – RRFQ: Basic Research Financing (Horizontal support for all Sciences)
Thematic area	ThA1. Physical Sciences, Engineering Sciences and Technology, Environment and Energy
Thematic Field	1.16 Smart Cities
Host Organization	Democritus University of Thrace
Collaborating Institutions	Aristotle University of Thessaloniki
Project starting date	13/3/2024
Project Principal Investigator	**Dr. Theodoros Rousakis**
Affiliation	**Democritus University of Thrace / Department of Civil Engineering**
Email	**trousak@civil.duth.gr**
Telephone	25410 79645, 461 / 6977421569
Deliverable number and title	**D4.1** Investigation of the scenario of high–rise renovated VF building subjected to multiple earthquakes and real time health monitoring
Related work package	**WP4** - Hybrid physical – digital testing platform and real time assessment of large scale VF buildings and multiple earthquakes scenario
Authors	Theodoros Rousakis, Vachan Vanian, Theodora Fanaradelli, Maristella Voutetaki, Adamantis Zapris (DUTh) Ifigeneia Theodoridou (AUTh)

Τίτλος Έργου	Ανθεκτική Αντισεισμική Ανακαίνιση Κατασκευών από Ωπλισμένο Σκυρόδεμα σε Κάθετο Δάσος
Ακρωνύμιο	GREENERGY
Αριθμός Έργου ΕΛΙΔΕΚ	015376
Δράση	Χρηματοδότηση Βασικής Έρευνας (Οριζόντια υποστήριξη όλων των Επιστημών), Εθνικό Σχέδιο Ανάκαμψης και Ανθεκτικότητας (Ελλάδα 2.0)
Θεματική Περιοχή	Υποδράση 2. Χρηματοδότηση Έργων σε Τομείς Αιχμής – ΤΑΑ: Χρηματοδότηση Βασικής Έρευνας (Οριζόντια υποστήριξη όλων των Επιστημών)
Θεματικό Πεδίο	1.16 Έξυπνες Πόλεις
Φορέας Υποδοχής	Δημοκρίτειο Πανεπιστήμιο Θράκης
Συνεργαζόμενος Φορέας	Αριστοτέλειο Πανεπιστήμιο Θεσσαλονίκης
Ημερομηνία έναρξης Έργου	13/3/2024
Επιστημονικά Υπεύθυνος Έργου	**Δρ. Θεόδωρος Ρουσάκης**
Ίδρυμα / Τμήμα	**Δημοκρίτειο Πανεπιστήμιο Θράκης / Πολιτικών Μηχανικών**
Email	**trousak@civil.duth.gr**
Τηλέφωνα	25410 79645, 461 / 6977421569
Αριθμός και Τίτλος Παραδοτέου	**D4.1** Διερεύνηση σεναρίου ανακαινισμένου πολυώροφου κτιρίου ΚΔ που υπόκειται σε πολλαπλούς σεισμούς και σύστημα παρακολούθησης της δομικής ακεραιότητας σε πραγματικό χρόνο.
Σχετική Ενότητα Εργασίας	**ΕΕ4** - Υβριδική φυσική-ψηφιακή πλατφόρμα δοκιμών και αξιολόγηση σε πραγματικό χρόνο κτιρίων ΚΔ μεγάλης κλίμακας και σεναρίου πολλαπλών σεισμών
Συγγραφείς	Θεόδωρος Ρουσάκης, Βαχάν Βανιάν, Θεοδώρα Φαναραδέλλη, Μαριστέλλα Βουτετάκη, Αδαμάντης Ζάπρης (ΔΠΘ) Ιφιγένεια Θεοδωρίδου (ΑΠΘ)

ACKNOWLEDGEMENTS

This project is carried out within the framework of the National Recovery and Resilience Plan Greece 2.0, funded by the European Union – NextGenerationEU (Implementation body HFRI).

TABLE OF CONTENTS

LIST OF TABLES

LIST OF FIGURES

ΠΕΡΙΛΗΨΗ

Η παρούσα ερευνητική έκθεση αξιολογεί την αντισεισμική συμπεριφορά μιας τυπικής υφιστάμενης εξαώροφης (πολυώροφης υψηλής) κατασκευής από οπλισμένο σκυρόδεμα (ΟΣ) που ανακαινίζεται με συστήματα Κάθετου Δάσους (VF), γλαστρών και Ζωντανών Τοίχων (LW). Χρησιμοποιώντας την υβριδική πλατφόρμα ReplicaXLite και το λογισμικό OpenSeesPy, η μελέτη διερευνά διάφορες δομικές παραλλαγές—συμπεριλαμβανομένων των pilotis και των πλαισίων με τοιχοπληρώσεις σε όλους τους ορόφους —υπό ιδιομορφική, Υπερωθητική Ανάλυση (στατική ανελαστική ανάλυση. Pushover) και δυναμική ανελαστική ανάλυση χρονοϊστορίας (Dynamic Time History Analysis). Δίνεται η δυνατότητα αξιοποίησης των πειραματικών αποτελεσμάτων σε σχέση με την επιτελεστικότητα των προηγμένων επεμβάσεων και της ανακαίνισης με κάθετα δάση (συνδυασμένη ανάλυση), σε υβριδική δοκιμή πολυώροφων κτηρίων για σενάρια διενέργειας πολλαπλών διεγέρσεων, με παρακολούθηση υγείας κατασκευής σε πραγματικό χρόνο. Η έρευνα στοχεύει στον προσδιορισμό του κατά πόσον οι εξειδικευμένες τεχνικές ενίσχυσης μπορούν να υποστηρίξουν με ασφάλεια την πρόσθετη υποδομή και μάζα των πράσινων παρεμβάσεων σε σενάρια σεισμών μακρινού και κοντινού πεδίου.

Λέξεις-κλειδιά: συνδυασμένη ανάλυση, υβριδική πλατφόρμα, δυναμική ανελαστική ανάλυση, κάθετη βλάστηση

SUMMARY

This report evaluates the seismic resilience of a typical six-story (multi-storey, high-rise) reinforced concrete (RC) structure renovated with Vertical Forest (VF), planters and Living Wall (LW) systems. Utilizing the ReplicaXLite hybrid platform and OpenSeesPy, the study investigates various structural configurations—including pilotis (soft-story) and infilled frames in all storeys—subjected to modal, non-linear static pushover, and dynamic inelastic time history analyses. The platform enables for the utilization of the experimental results with respect to the performance of advanced interventions and vertical forest renovations (coupled analysis), in hybrid testing of high-rise buildings for executing multiple earthquake scenarios, with real-time health monitoring. The research aims to determine if specialized retrofitting-strengthening techniques can safely support the additional infrastructure and mass of green interventions under both far-field and aggressive near-field seismic scenarios.

Keywords: coupled analysis, hybrid platform, dynamic inelastic analysis, vertical greenery

1 INTRODUCTION

The use of specialized software to investigate the behavior of structural components, systems, or entire structures under varying loading conditions has been achieved in the past using the OpenSees solver as the computational engine. FeView (Rahman et al., 2021) is an open-source, Python-based graphical user interface (GUI) tool for OpenSees, designed to visualize finite element models (FEM) and perform post-processing tasks such as contour plots, nodal response graphs, and response spectrum analysis. It supports 46 element types, diverse material models, and integrates with Tcl scripting for model definition, offering real-time visualization via PyVista and compatibility with OpenSees' analysis capabilities. However, its limitations include the absence of built-in pre-processing tools, requiring users to manually create Tcl files.

The initial and current state of OpenSeesPyView (Guo et al., 2023) primarily focuses on visualization and post-processing, rather than providing a complete, user-friendly pre-processing (model generation) GUI. GiD+OpenSees Interface (Papanikolaou et al., 2017) is an open-source add-on that connects the OpenSees solver with the general graphical pre/post-processor GiD. It allows users to create model geometry, assign materials and boundary conditions, select analysis options, and visualize results within the GiD environment, making the code-based modeling process more accessible. To use the interface, users need the GiD software, which is a commercial product and may incur licensing costs, even though the OpenSees add-on itself is open-source.

opstool (Yan & Xie, 2025) is an open-source Python library designed to enhance OpenSeesPy by automating pre- and post-processing tasks, streamlining data management, and enabling advanced visualization. It integrates tools like xarray for structured data handling, PyVista and Plotly for 3D/interactive visualizations, and adaptive algorithms to improve convergence in nonlinear analyses. The package simplifies workflows for finite element modeling, supports modal and dynamic response analysis, and facilitates comparison with commercial software like SAP2000.

The opstool capabilities were used to create the ReplicaXLite hybrid platform to provide nearly real-time integration of sensor processing and Finite Element Analysis (FEA) using OpenSeesPy (a Python wrapper around the Tcl OpenSees version) as the solver engine, with the seismic table (and additional material and component testing facilities) at the Reinforced Concrete and Seismic Design of Structures Laboratory at Democritus University of Thrace, Xanthi, Greece. The ReplicaXLite package contains four distinct APIs that enable the hybrid platform to operate in a CLI (Command Line Interface) environment for advanced analyses that require deep understanding of the package, civil engineering practices, FEA, and Python programming. For new users, a detailed GUI analysis is also provided with terminal integration for user-friendly learning and analysis that integrates all four APIs.

The core API is the Structural API, which creates the digital twin model, performs the analysis, and saves the results in a permanent database for later post-processing. The second important API is the SensorAPI, which primarily reads the sensors' raw data and makes the necessary adjustments so that it makes physical sense and is ready to be compared with the numerical results. It can also send edited data back to the original mechanical components or other devices, as it supports the CSV export format. The third API is the Converter API, which helps convert quantities between different unit systems. The last API is the DataValidation API, which is primarily for internal data validation but can also be used for any other suitable case.

This report presents the results from the modal analysis of several configurations of a six-storey structure: Bare Frame + Infill + Pilotis (BFIP), Bare Frame + Infill (BFI), Bare Frame + Infill + Pilotis + Retrofit (BFIPR), Bare Frame + Infill + Retrofit (BFIR), SBFI (Strong Bare Frame +infill) and SBFIR (Strong Bare Frame + Infill + Retrofit). This specific building height was selected as it represents the majority of existing high-rise multi-storey buildings in Thessaloniki and offers a case of extended available surface area for vertical greenery interventions.

These building types were tested using coupled (structural and greenery) pushover and dynamic inelastic analyses. The dynamic analyses were conducted for: a) near-field earthquakes, based on the Kobe earthquake (a 0.4 scaled version of the Kobe earthquake); and b) far-field earthquake based on Thessaloniki 1978 excitation. For the latter, a dynamic push over approach with multiple excitations, using the 1978 Thessaloniki earthquake with a maximum intensity of 0.5g was employed. The analyses assess the proposed retrofitting-strengthening techniques with respect to the damage prevention to infills, following the addition of infrastructure and mass from Vertical Living Walls and Planters (Vertical Forests) in buildings with adequate seismic capacity to withstand far-field earthquakes. Furthermore, the study investigates the performance of an existing building with stronger RC frame and thicker infills and with higher thickness seismic joints up to the top floor, when subjected to a near-field earthquake of up to 40% of the intensity of the Kobe earthquake.

A comparison of the analyses results is conducted in the Conclusion section. Finally, an integration of sensors for real time structural health monitoring and integration with other machines is provided to prove the concept of the advanced hybrid platform.

2 3D STRUCTURE MODELING

2.1 CURRENT INFILL MODELING

In the current research the modeling approach for the unreinforced infills (see also D32 (Rousakis et al., 2025)) follows the one proposed by (Di Trapani et al., 2018) and was modified by (Pradhan & Cavaleri, 2020). The main changes that the later research implemented were to replace the pin-connected end conditions with fixed-end connections (this modification was implemented to limit excessive mid-span deflections and enhance the arching mechanism under out-of-plane loading conditions) for all struts and to adopt unified material properties for all infill elements (adopting a single effective compressive strength value for defining the compressive behavior of all struts, thereby reducing the complexity of parameter calibration). See Figure 1 for more details. The modified model utilizes surrogate thickness values for all struts (diagonal, horizontal, and vertical). This ensures consistent cross-sectional treatment across all equivalent strut elements. While the original model relied on empirical assignment of mechanical characteristics (deformation at peak strength ε_o, ultimate strength f_{mu}, and ultimate strain ε_{mu}) without systematic procedures, the modified model introduces a standardized methodology for deriving these parameters through correlation equations based on the actual mechanical properties of the masonry infill.

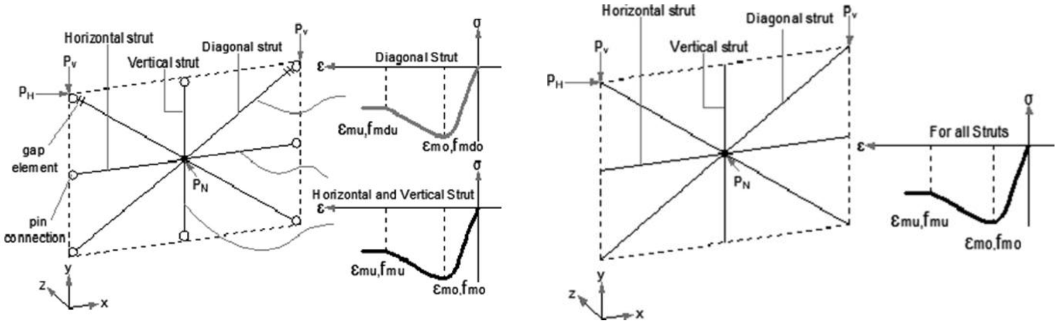

a) b)

Figure 1 Proposed model from a) (Di Trapani et al., 2018) and b) (Pradhan & Cavaleri, 2020) adapted from (Pradhan & Cavaleri, 2020)

The mass application in the proposed modified four-strut macro model centers on four mid-span nodes located at the geometric center of the infill panel, positioned at the intersection of the diagonal, horizontal, and vertical struts. The total mass of the infill wall is concentrated at these four central nodes using a lumped mass approach, which simplifies dynamic analysis while maintaining sufficient accuracy for practical engineering applications. The critical aspect of this mass system is the constraint mechanism governing these mass-bearing nodes. Each of the four mid-span nodes can exhibit different displacements in the plane of the infill (allowing for complex stress distributions during in-plane loading), but they are rigidly connected in the out-of-plane direction, ensuring the entire infill mass moves as a cohesive unit when subjected to lateral loads perpendicular to the wall plane. This constraint system enables the model to capture the arching mechanism that develops in masonry infills under OOP loading, where mass distribution and inertial effects are crucial. The practical application involves applying OOP loads directly to these central mass nodes, as described in the validation studies where "the OOP load was applied at the center of the struts representing the infill center." This loading approach ensures that applied forces are transmitted through the constraint system to all four struts simultaneously, activating the bending response in the fiber-section beam-column elements. While the paper doesn't provide explicit mass distribution equations, the approach assumes the total infill mass is equally distributed among the four central nodes, consistent with the macro-modeling philosophy that prioritizes computational efficiency for large-scale structural analysis.

H.F.R.I. Hellenic Foundation for Research & Innovation — Greece 2.0 NATIONAL RECOVERY AND RESILIENCE PLAN — Funded by the European Union NextGenerationEU — GREENERGY

Modified Four-Strut Macro Model for URM Infilled Frames
Pradhan & Cavaleri (2020) - Engineering Structures 224

1. Input Parameters

Geometry:

- l, h = clear length/height
- l', h' = center distances
- t = infill thickness

Materials:

- fm1, fm2 = compressive strength
- Em1, Em2 = elastic moduli

Table 1, Page 4

2. Equivalent Properties

```
Eq. (9a): fm = sqrt(fm1 x fm2)
Eq. (9b): Em = sqrt(Em1 x Em2)
```

For solid units: fm1 = fm2, Em1 = Em2

Page 6-7

↓

3. Basic Strut Dimensions

```
Eq. (1a): d = sqrt(l'^2 + h'^2)
wd = d/3
Eq. (1b): wh = h - (wd/cos_theta)
Eq. (1c): wv = l - (wd/sin_theta)
```

Equations (1a-1c), Page 3; Figure 6

↓

4. Empirical Parameters (Correlation Method)

```
Calculate: fmEm = fm × Em
```

```
Eq. (10): fmo = {
  0.61+0.0001fmEm x 10^-9(fmEm)^2, if fmEm<40000
  3, if fmEm>=40000
```

```
Eq. (11): eps_mo = 4 x 10^-8 fmEm + 0.00039
```

```
Eq. (12): eps_mu = {
  0.0047+4 x 10^-7 fmEm-3 x 10^-12(fmEm)^2, if fmEm<48000
  0.017, if fmEm>=48000
```

fmu = 60% of fmo (Page 8)

Equations (10-12), Pages 11-12

↓

5. Surrogate Dimensions

```
Eq. (8a): w_surr = sqrt(fmo/fm) x w
Eq. (8b): t_surr = sqrt(fm/fmo) x t
Constraint Eq. (6): wt = w_surr x t_surr
```

Maintains same cross-sectional area

Equations (6), (8a-8b), Page 6

↓

6. Model Configuration

Four-Strut System:

- 2 diagonal + 1 horizontal + 1 vertical
- Each: 2 fiber-section beam elements
- Connected at mid-span nodes

Key Modifications:

- All struts use surrogate thickness
- End connections: rotation restrained
- Single fmo value for all struts

Section 2, Pages 3-4; Figure 5

Figure 2 Summary workflow for infill parameters identification based on (Pradhan & Cavaleri, 2020)

2.2 MASS DISTRIBUTION

The structural mass for each case is calculated using the seismic combination G+0.3Q. The permanent load (G) is derived from the self-weight of structural components—such as reinforced concrete elements, infills, living walls, and vertical forests—based on the specific structure type examined. The live load (Q) is derived from loads of 2 kN/m² or 5 kN/m² applied to the slabs. Specifically, cantilevers are assigned a load of 5 kN/m², while the remaining areas are assigned 2 kN/m². Additional permanent loads are calculated as a proportion of the uniform load on the slabs. To simplify calculations, permanent loads are separated into self-weight and a G+0.3Q combination derived solely from the uniform slab loads. As with the small-scale models developed in Deliverable 3.2 (Rousakis, et al., 2025), the mass is distributed as lumped masses at the edges of the vertical components, concentrated at the center of the infills, and equally distributed across the five nodes of each living wall. The mass properties for the far-field earthquake case are presented in Table 1, Table 2, Table 3, Table 4, Table 5 and Table 6. The mass distribution is categorized into 'RC frame' (representing the self-weight of beams, columns, and slabs) and 'RC Frame G+0.3Q' (accounting for additional permanent and live loads). This same approach is applied to the cantilever calculations. For the near-field earthquake analysis, the mass properties of the first floor are applied to all upper floors, as the cross-sections and floor usage remain unchanged.

Table 1 Mass for RC structure for floor 1.

Column Node	RC frame (tonne)	RC Frame G+0.3Q (tonne)	Cantilevers (tonne)	Cantilevers G+0.3Q (tonne)
1036	4.73	0.93	0.98	0.46
1037	6.77	1.34	1.01	0.67
1038	6.77	1.34	1.01	0.67
1039	4.73	0.93	0.98	0.46
1040	7.68	1.86	0.00	0.00
1041	10.59	2.68	0.00	0.00
1042	10.59	2.68	0.00	0.00
1043	7.68	1.86	0.00	0.00
1044	4.73	0.93	0.98	0.46
1045	6.77	1.34	1.01	0.67
1046	6.77	1.34	1.01	0.67
1047	4.73	0.93	0.98	0.46
1065	0.00	0.00	0.98	0.46
1066	0.00	0.00	1.40	0.67
1067	0.00	0.00	1.40	0.67
1068	0.00	0.00	0.98	0.46
1069	0.00	0.00	0.98	0.46
1070	0.00	0.00	1.40	0.67
1071	0.00	0.00	1.40	0.67
1072	0.00	0.00	0.98	0.46
Total	127.31			

Table 2 Mass for RC structure for floor 2.

Column Node	RC frame (tonne)	RC Frame G+0.3Q (tonne)	Cantilevers (tonne)	Cantilevers G+0.3Q (tonne)
2036	4.73	0.93	0.98	0.46
2037	6.77	1.34	1.01	0.67
2038	6.77	1.34	1.01	0.67
2039	4.73	0.93	0.98	0.46
2040	7.68	1.86	0.00	0.00
2041	10.59	2.68	0.00	0.00
2042	10.59	2.68	0.00	0.00
2043	7.68	1.86	0.00	0.00
2044	4.73	0.93	0.98	0.46
2045	6.77	1.34	1.01	0.67
2046	6.77	1.34	1.01	0.67
2047	4.73	0.93	0.98	0.46
2065	0.00	0.00	0.98	0.46
2066	0.00	0.00	1.40	0.67
2067	0.00	0.00	1.40	0.67
2068	0.00	0.00	0.98	0.46
2069	0.00	0.00	0.98	0.46
2070	0.00	0.00	1.40	0.67
2071	0.00	0.00	1.40	0.67
2072	0.00	0.00	0.98	0.46
Total	127.31			

Table 3 Mass for RC structure for floor 3.

Column Node	RC frame (tonne)	RC Frame G+0.3Q (tonne)	Cantilevers (tonne)	Cantilevers G+0.3Q (tonne)
3036	4.46	0.93	0.98	0.46
3037	6.49	1.34	1.01	0.67
3038	6.49	1.34	1.01	0.67
3039	4.46	0.93	0.98	0.46
3040	7.41	1.86	0.00	0.00
3041	10.31	2.68	0.00	0.00
3042	10.31	2.68	0.00	0.00
3043	7.41	1.86	0.00	0.00
3044	4.46	0.93	0.98	0.46
3045	6.49	1.34	1.01	0.67

Column Node	RC frame (tonne)	RC Frame G+0.3Q (tonne)	Cantilevers (tonne)	Cantilevers G+0.3Q (tonne)
3046	6.49	1.34	1.01	0.67
3047	4.46	0.93	0.98	0.46
3065	0.00	0.00	0.98	0.46
3066	0.00	0.00	1.40	0.67
3067	0.00	0.00	1.40	0.67
3068	0.00	0.00	0.98	0.46
3069	0.00	0.00	0.98	0.46
3070	0.00	0.00	1.40	0.67
3071	0.00	0.00	1.40	0.67
3072	0.00	0.00	0.98	0.46
Total	124.0			

Table 4 Mass for RC structure for floor 4.

Column Node	RC frame (tonne)	RC Frame G+0.3Q (tonne)	Cantilevers (tonne)	Cantilevers G+0.3Q (tonne)
4036	4.46	0.93	0.98	0.46
4037	6.49	1.34	1.01	0.67
4038	6.49	1.34	1.01	0.67
4039	4.46	0.93	0.98	0.46
4040	7.41	1.86	0.00	0.00
4041	10.31	2.68	0.00	0.00
4042	10.31	2.68	0.00	0.00
4043	7.41	1.86	0.00	0.00
4044	4.46	0.93	0.98	0.46
4045	6.49	1.34	1.01	0.67
4046	6.49	1.34	1.01	0.67
4047	4.46	0.93	0.98	0.46
4065	0.00	0.00	0.98	0.46
4066	0.00	0.00	1.40	0.67
4067	0.00	0.00	1.40	0.67
4068	0.00	0.00	0.98	0.46
4069	0.00	0.00	0.98	0.46
4070	0.00	0.00	1.40	0.67
4071	0.00	0.00	1.40	0.67
4072	0.00	0.00	0.98	0.46

Column Node	RC frame (tonne)	RC Frame G+0.3Q (tonne)	Cantilevers (tonne)	Cantilevers G+0.3Q (tonne)
Total	124.0			

Table 5 Mass for RC structure for floor 5.

Column Node	RC frame (tonne)	RC Frame G+0.3Q (tonne)	Cantilevers (tonne)	Cantilevers G+0.3Q (tonne)
5036	3.98	0.93	0.93	0.46
5037	5.82	1.34	1.01	0.67
5038	5.82	1.34	1.01	0.67
5039	3.98	0.93	0.93	0.46
5040	6.78	1.86	0.00	0.00
5041	9.51	2.68	0.00	0.00
5042	9.51	2.68	0.00	0.00
5043	6.78	1.86	0.00	0.00
5044	3.98	0.93	0.93	0.46
5045	5.82	1.34	1.01	0.67
5046	5.82	1.34	1.01	0.67
5047	3.98	0.93	0.93	0.46
5065	0.00	0.00	0.93	0.46
5066	0.00	0.00	1.34	0.67
5067	0.00	0.00	1.34	0.67
5068	0.00	0.00	0.93	0.46
5069	0.00	0.00	0.93	0.46
5070	0.00	0.00	1.34	0.67
5071	0.00	0.00	1.34	0.67
5072	0.00	0.00	0.93	0.46
Total	115.88			

Table 6 Mass for RC components for floor 6

Column Node	RC frame (tonne)	RC Frame G+0.3Q (tonne)	Cantilevers (tonne)	Cantilevers G+0.3Q (tonne)
6036	3.98	0.93	0.93	0.46
6037	5.82	1.34	1.01	0.67
6038	5.82	1.34	1.01	0.67
6039	3.98	0.93	0.93	0.46
6040	6.78	1.86	0.00	0.00
6041	9.51	2.68	0.00	0.00

H.F.R.I. Hellenic Foundation for Research & Innovation
Greece 2.0 NATIONAL RECOVERY AND RESILIENCE PLAN
Funded by the European Union NextGenerationEU
GREENERGY

Column Node	RC frame (tonne)	RC Frame G+0.3Q (tonne)	Cantilevers (tonne)	Cantilevers G+0.3Q (tonne)
6042	9.51	2.68	0.00	0.00
6043	6.78	1.86	0.00	0.00
6044	3.98	0.93	0.93	0.46
6045	5.82	1.34	1.01	0.67
6046	5.82	1.34	1.01	0.67
6047	3.98	0.93	0.93	0.46
6065	0.00	0.00	0.93	0.46
6066	0.00	0.00	1.34	0.67
6067	0.00	0.00	1.34	0.67
6068	0.00	0.00	0.93	0.46
6069	0.00	0.00	0.93	0.46
6070	0.00	0.00	1.34	0.67
6071	0.00	0.00	1.34	0.67
6072	0.00	0.00	0.93	0.46
Total	115.88			

For each vertical forest, trees are assumed to have the mass of young olive trees with a total height of 1.5 m (0.9 m for the trunk and 0.6 m for the crown). Crown mass is assumed to be 20 kg. The modeling approach follows methodology c) from (Vanian et al., 2025) as depicted in Figure 1. Each pod is assumed to weigh 153 kg (Rousakis et al., 2025). The total amount of mass accounts to 8.31 tonnes.

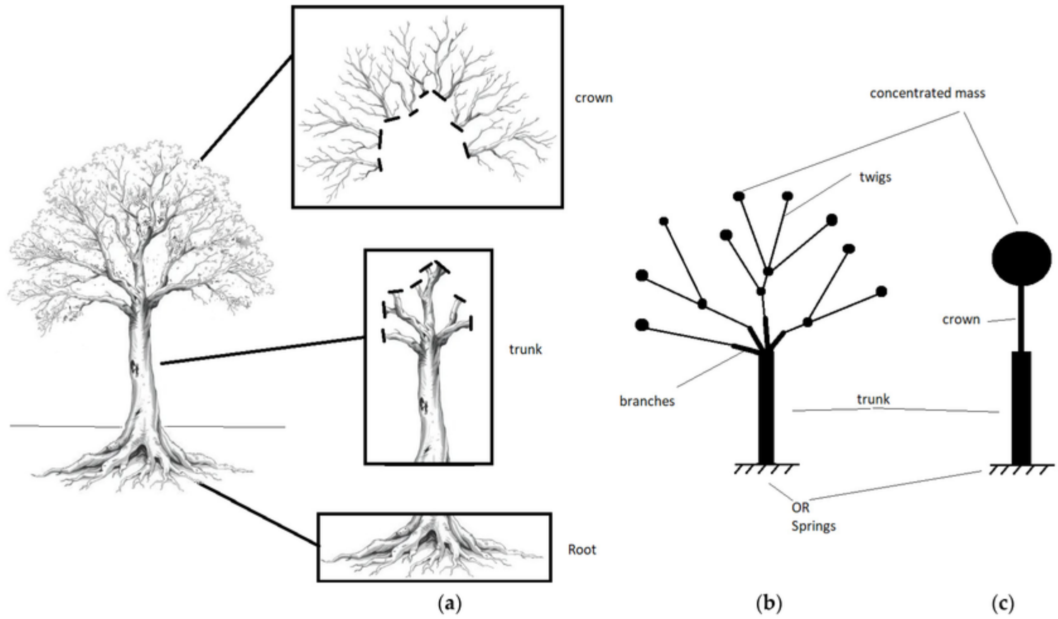

Figure 3 Finite element method (FEM) modeling approaches for tree structures, showing increasing levels of abstraction from left to right. (a) High-fidelity 3D model. (b) Simplified branch-mass model. (c) Equivalent two-element model. (adapted from (Vanian et al., 2025))

For the living walls, the lumped mass was distributed across the five nodes based on a weight of 40 kg/m², distributed over an area of 3 m by 2.25 m, covering a total surface area of 162 m² at each building face (both faces-sides are covered). Therefore, the total mass of the living walls is 12.96 tonnes. Finally, the total mass of infills when all are enabled in the model is 58.5 tonnes in case of the far-field moderate earthquake for the light brick infill scenario and 233.95 tonnes for the strong (heavy) brick infill scenario (4x, as the thickness of the infill is increased four times, equal to 24 cm) in case of the near-field severe earthquake.

2.3 STRUCTURAL COMPONENT CROSS-SECTION DEFINITION

The cross-section definitions are derived from the study by (Nafeh & O'Reilly, 2022). The plan for each floor and the corresponding cross-sections are depicted in Figure 4 through Figure 11. Figure 4 illustrates the cross-sectional details for three different floor groups: a) Floors 1 and 2, b) Floors 3 and 4, and c) Floors 5 and 6. The structural system consists of a regular grid layout with columns positioned at the intersections of gridlines A, B, and C (longitudinal) and gridlines 1, 2, 3, and 4 (transverse), spanning a total plan dimension of 11.0 m × 9.0 m. The reinforcement of the cross-sections is assumed to be smooth with a grade similar to S400, and the concrete is defined as in Deliverable 3.2 (Rousakis, et al., 2025). Column sizes vary by floor level: C35×35 sections are used on the ground and lower floors (Floors 1 and 2), C30×30 sections are employed on the middle floors (Floors 3 and 4), and C25×25 sections are utilized on the upper floors (Floors 5 and 6). The beam sections also vary, with B30×50 and B30×70 beams used on Floors 1 through 4, and B25×50 and B25×70 beams used on Floors 5 and 6. The specific beam dimensions depend on their position in the structural grid. Slab positions are indicated by circular markers labeled '(d=17)' distributed throughout the floor plans. The structural layout includes cantilever extensions of 1.5 m on the horizontal edges, as indicated in Figure 5 through Figure 11. For the near-field earthquake case, the cross-sections of Floor 1 are repeated up to the top floor level.

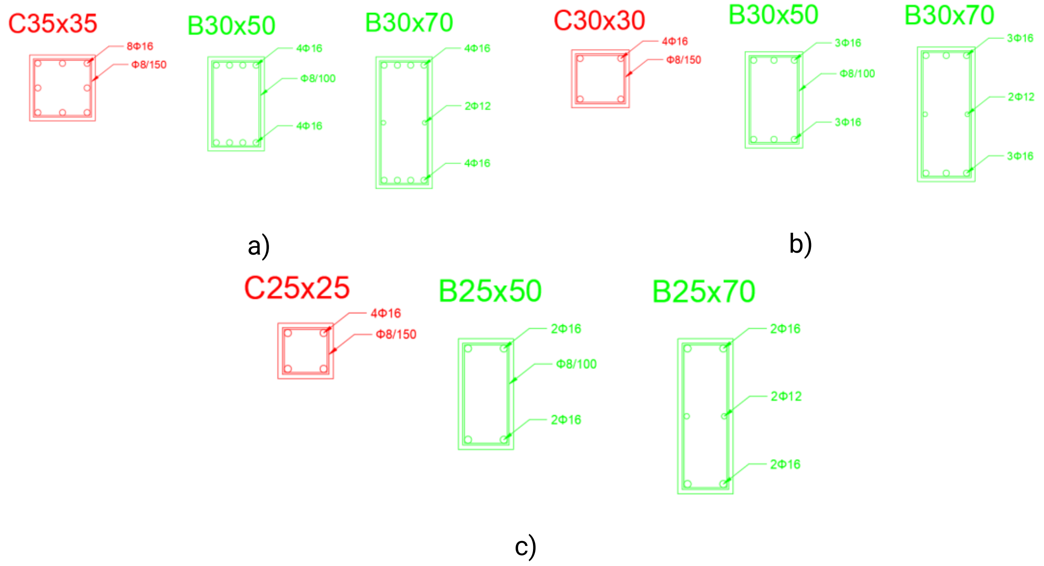

Figure 4 Cross-Section for a) Floor 1 and Floor2, b) Floor 3 and Floor 4 and c) Floor 5 and Floor 6.

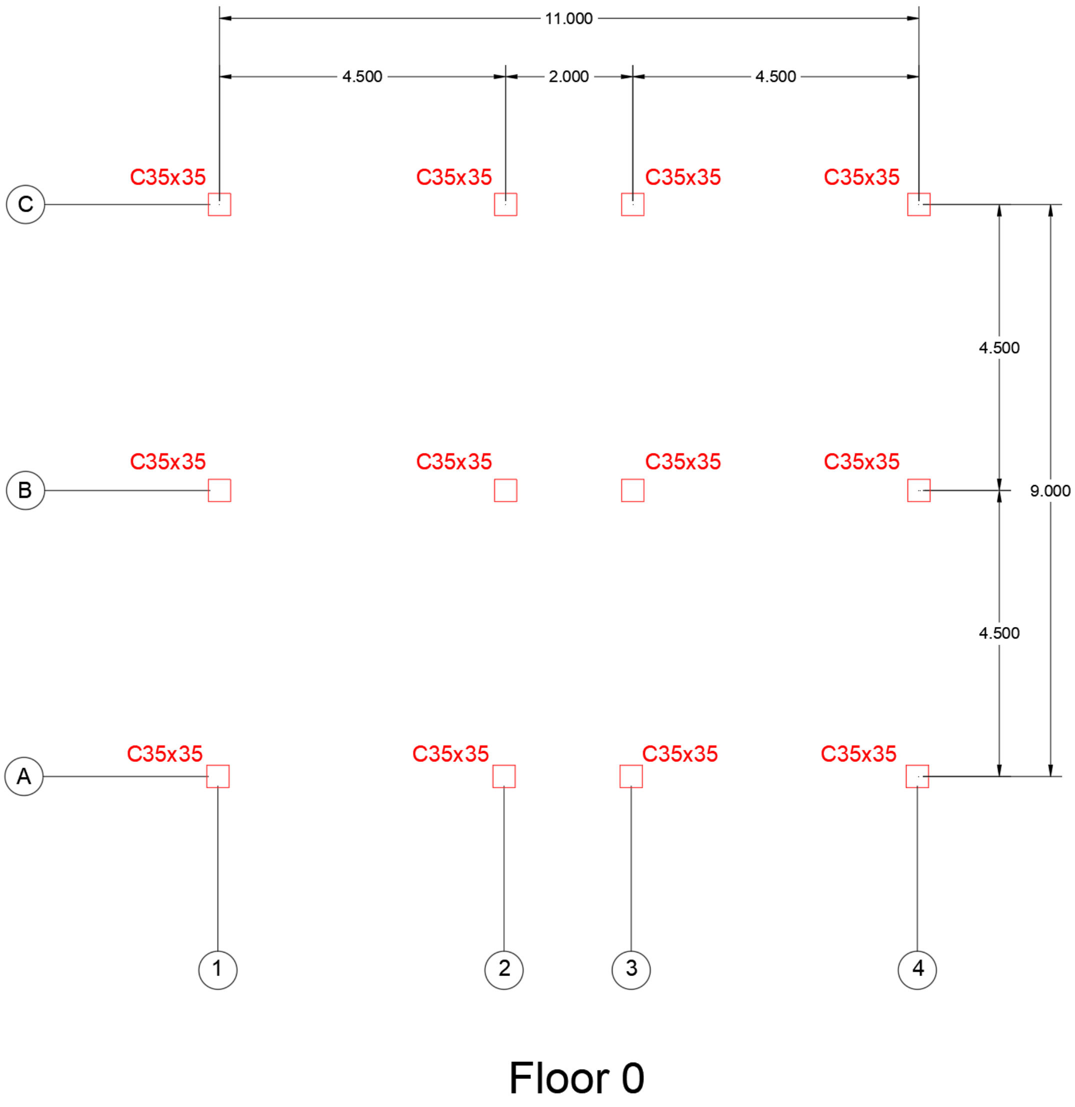

Figure 5 Plan of level 0.

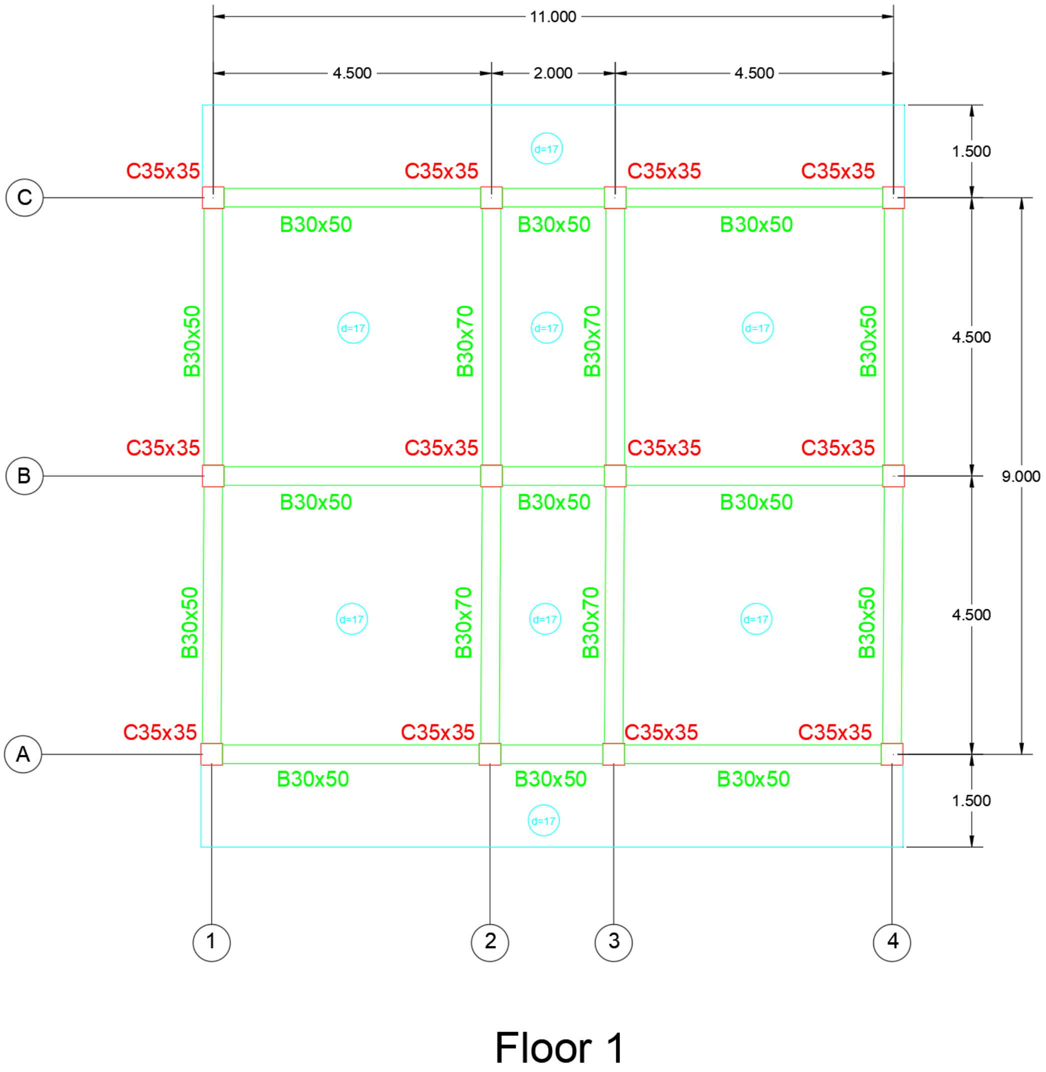

Figure 6 Plan of level 1.

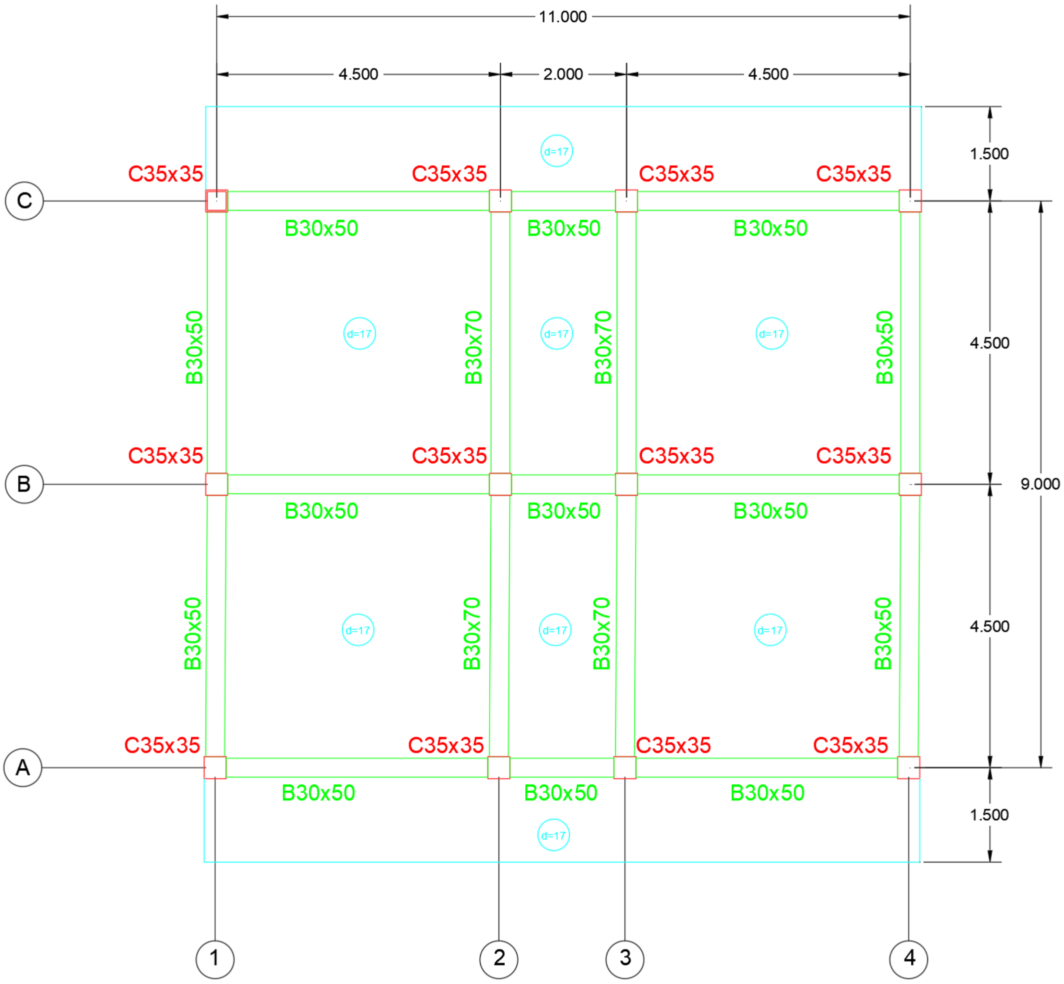

Floor 2

Figure 7 Plan of level 2.

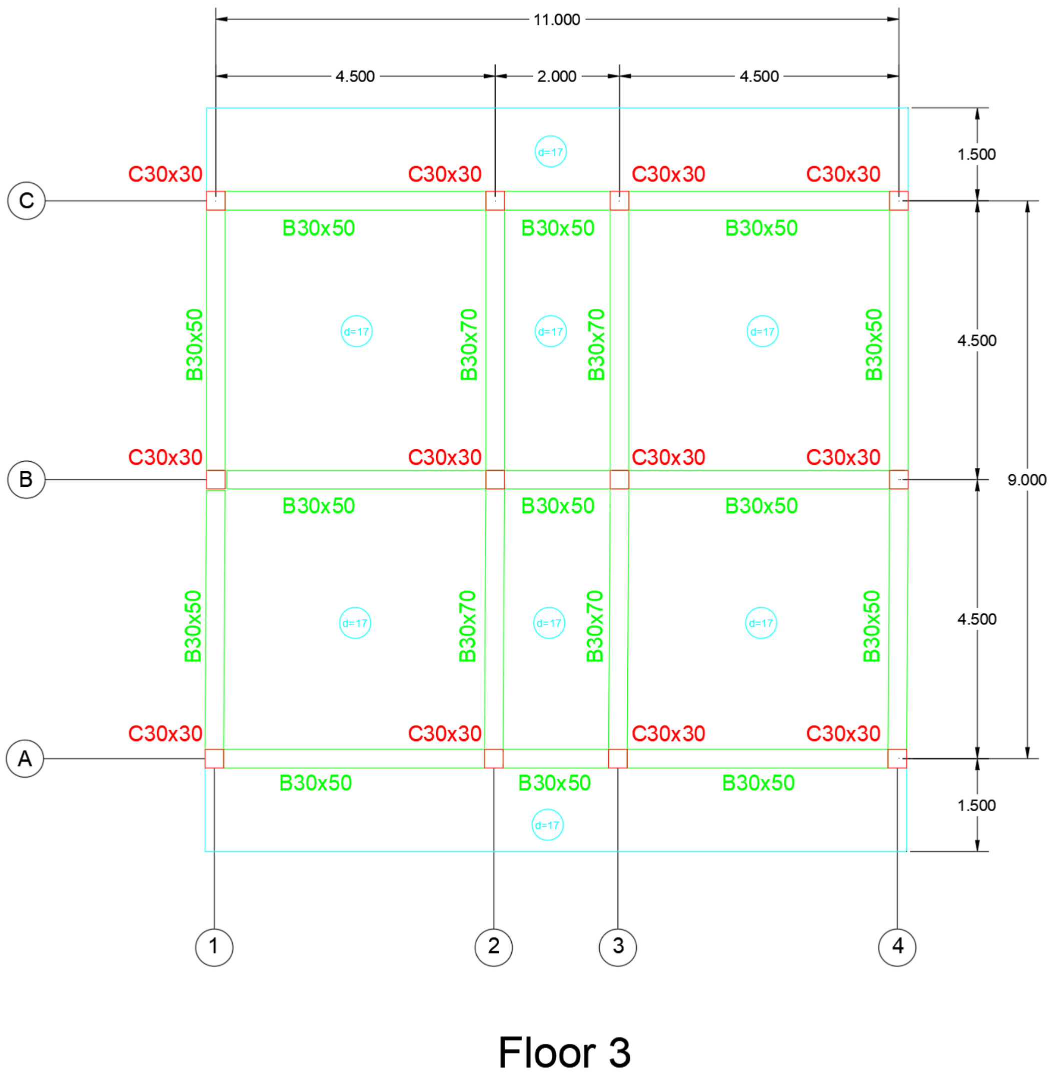

Figure 8 Plan of level 3.

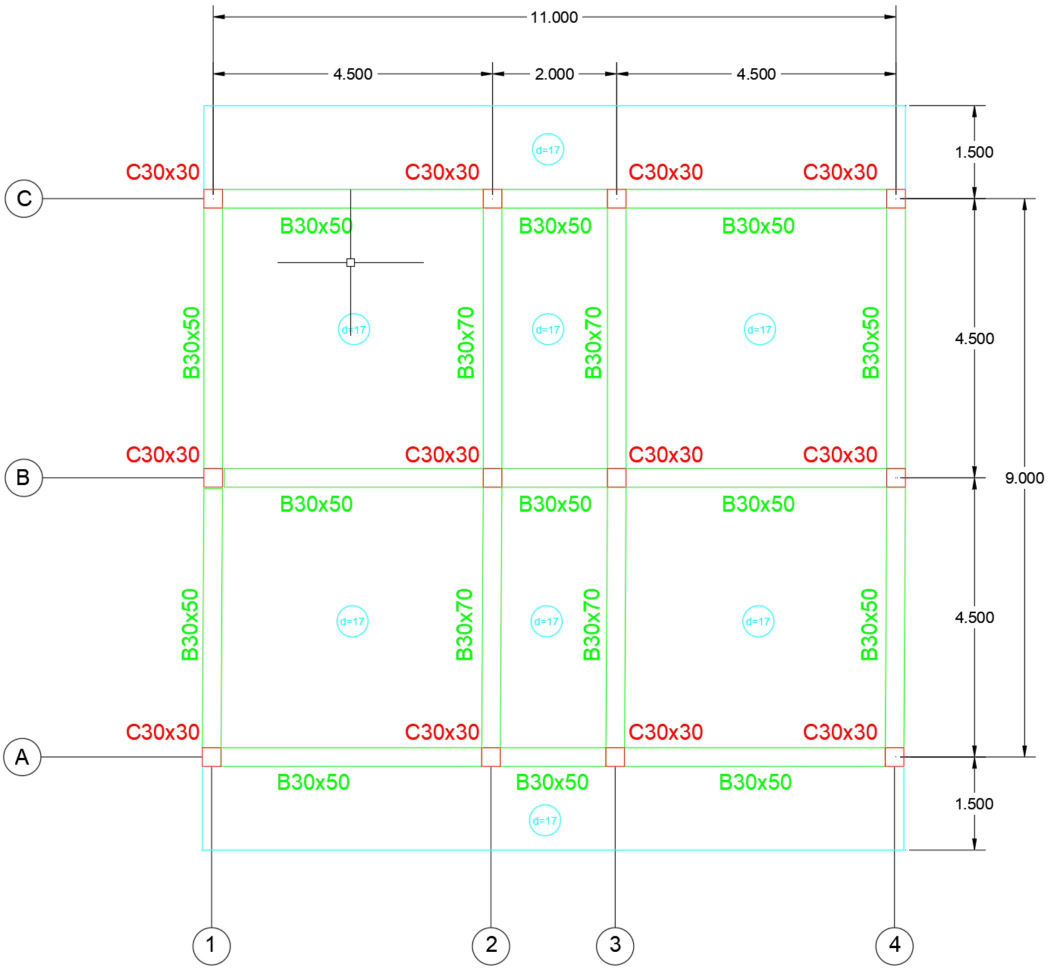

Floor 4

Figure 9 Plan of level 4.

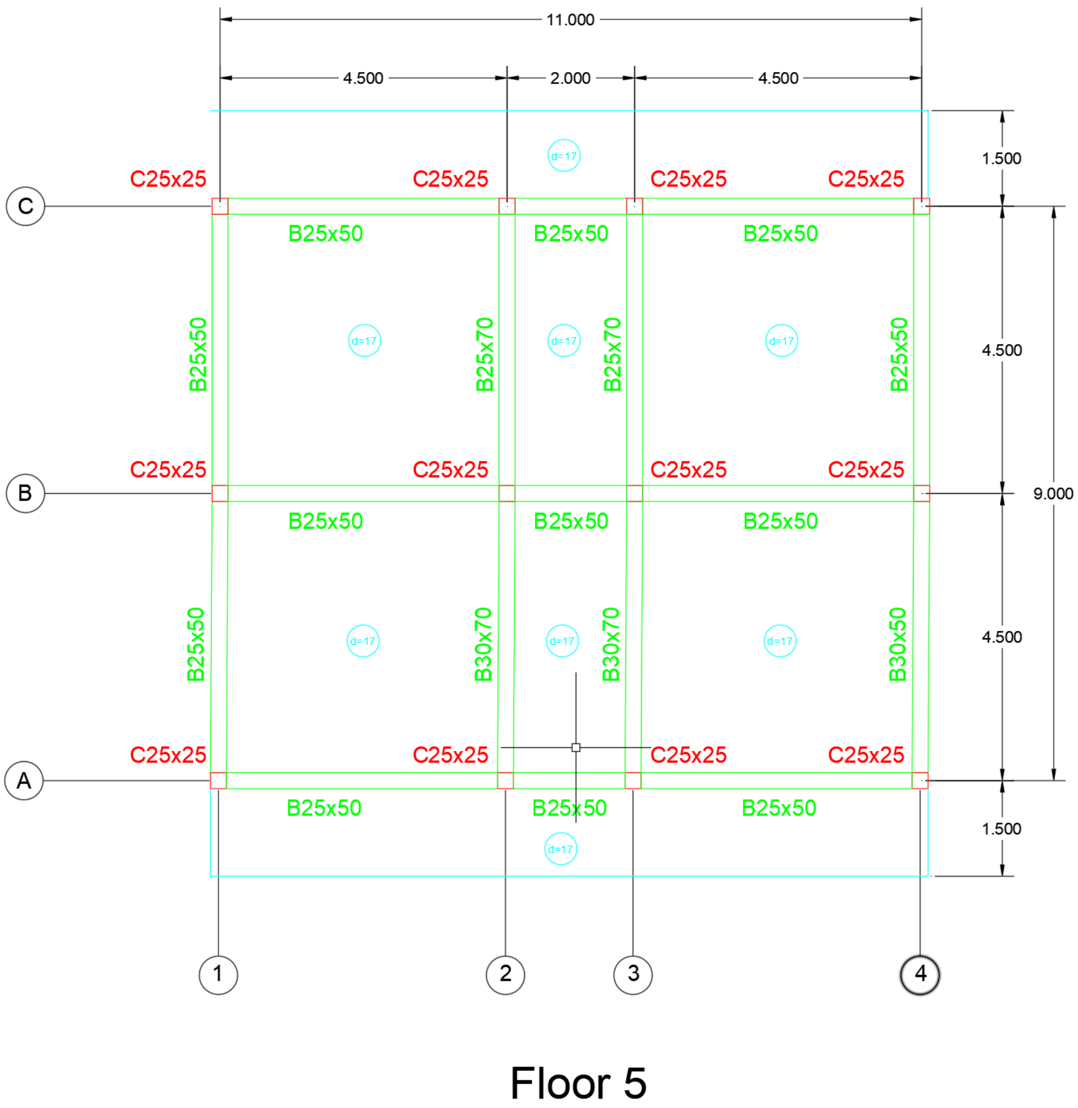

Figure 10 Plan of level 5.

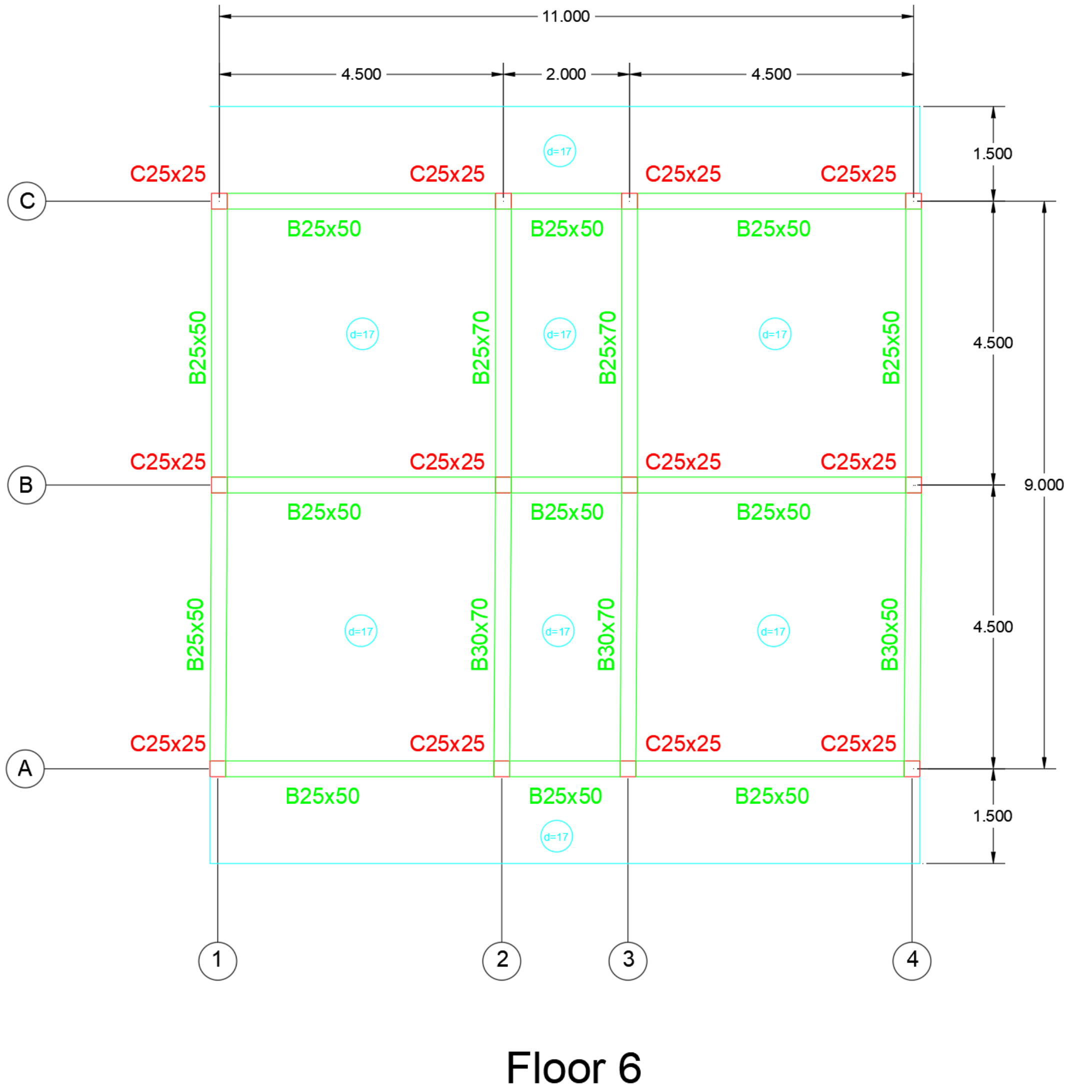

Figure 11 Plan of level 6.

2.4 CONSTRAINTS AND GRAVITY LOADS

The spatial representation of the bare frame—including the addition of infills, PUFJ, FRPU, basalt ropes, planters with trees and vertical living walls (vertical forest)—along with their associated constraints, is presented in Figure 12, Figure 13, Figure 14, Figure 15 and Figure 16. These are illustrated as combinations of the bare frame and specific interventions to facilitate easy inspection, while the final figure depicts the fully integrated structure.

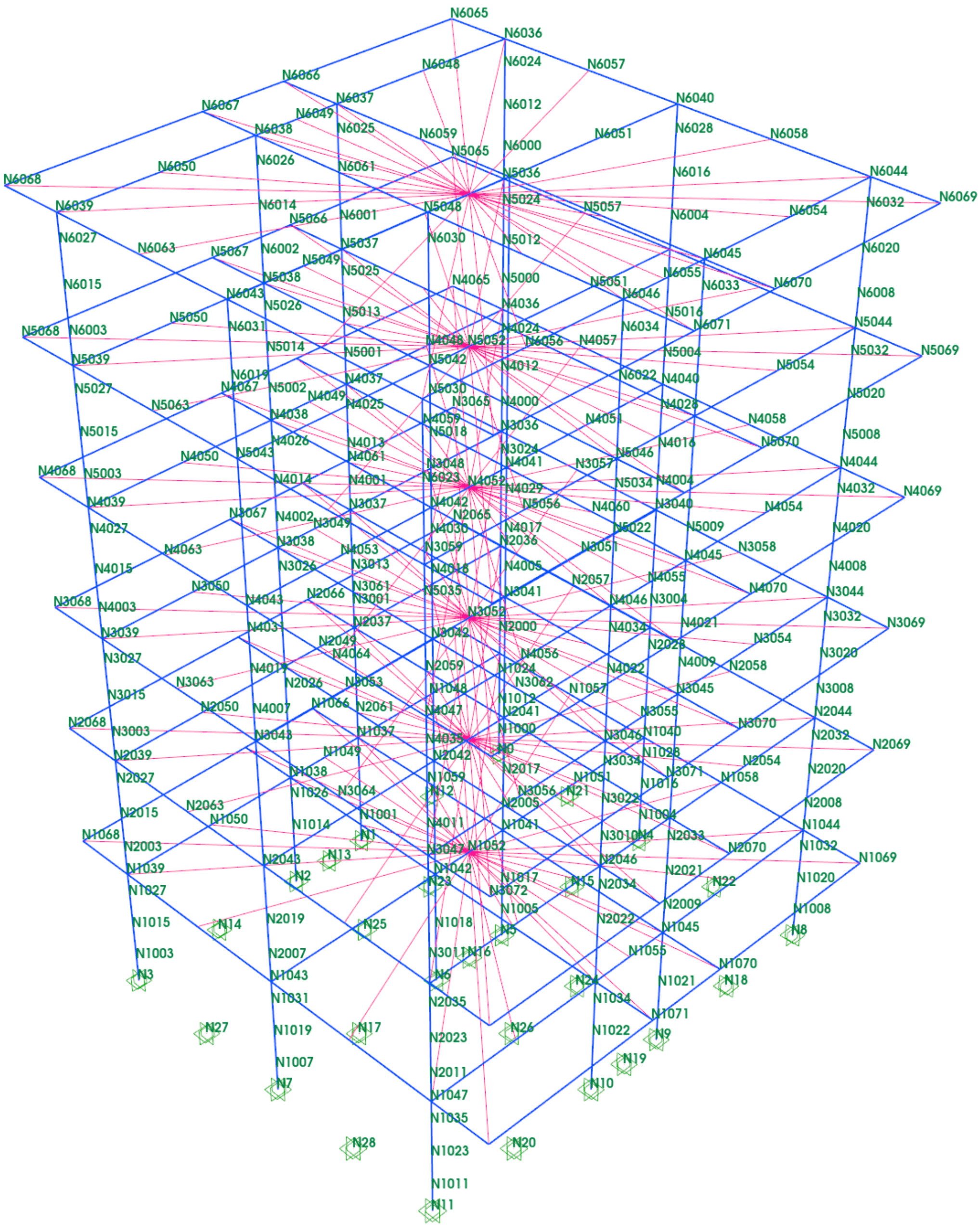

Figure 12 Spatial representation of the Bare frame structure.

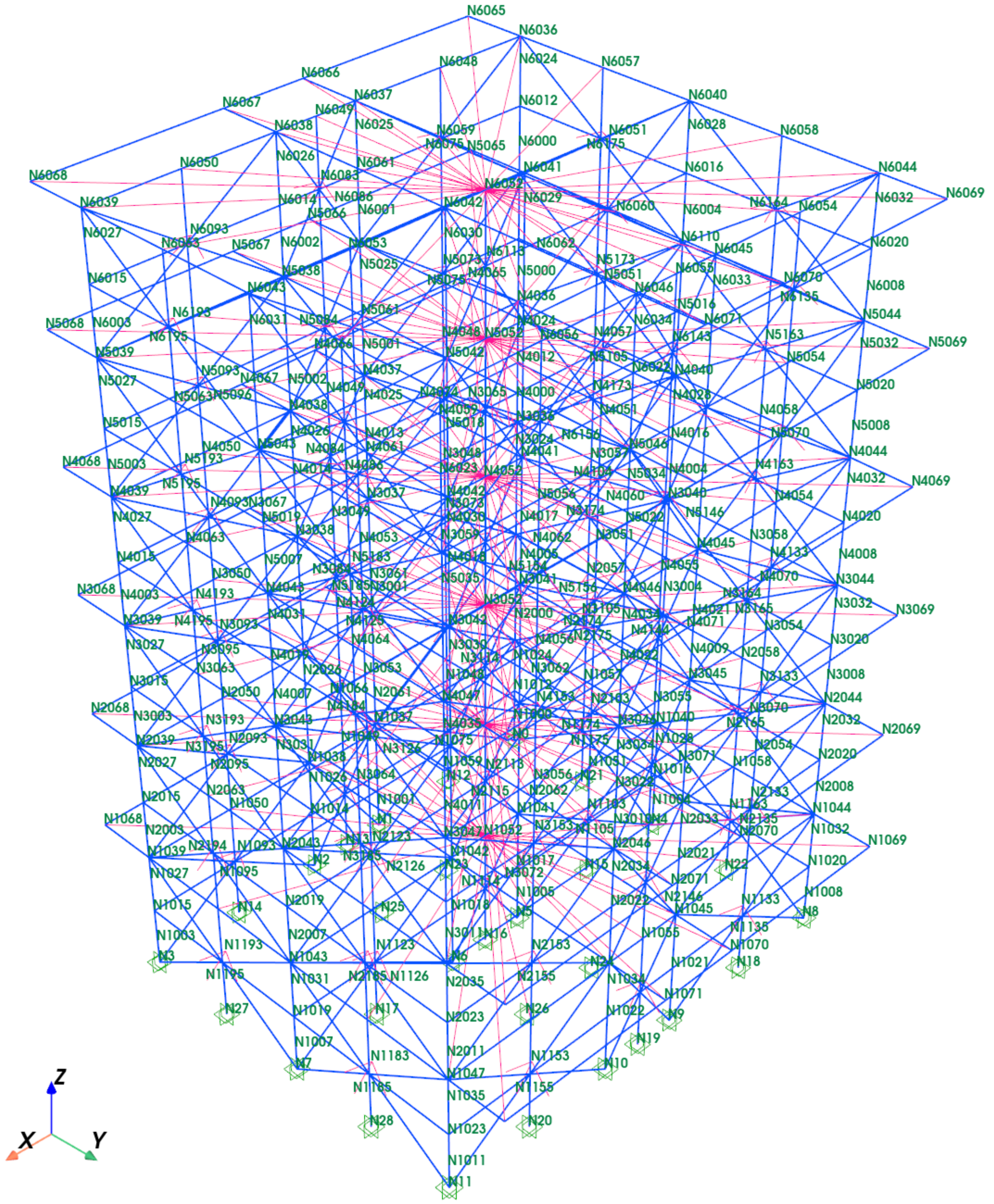

Figure 13 Spatial representation of the Bare frame structure with infills enabled.

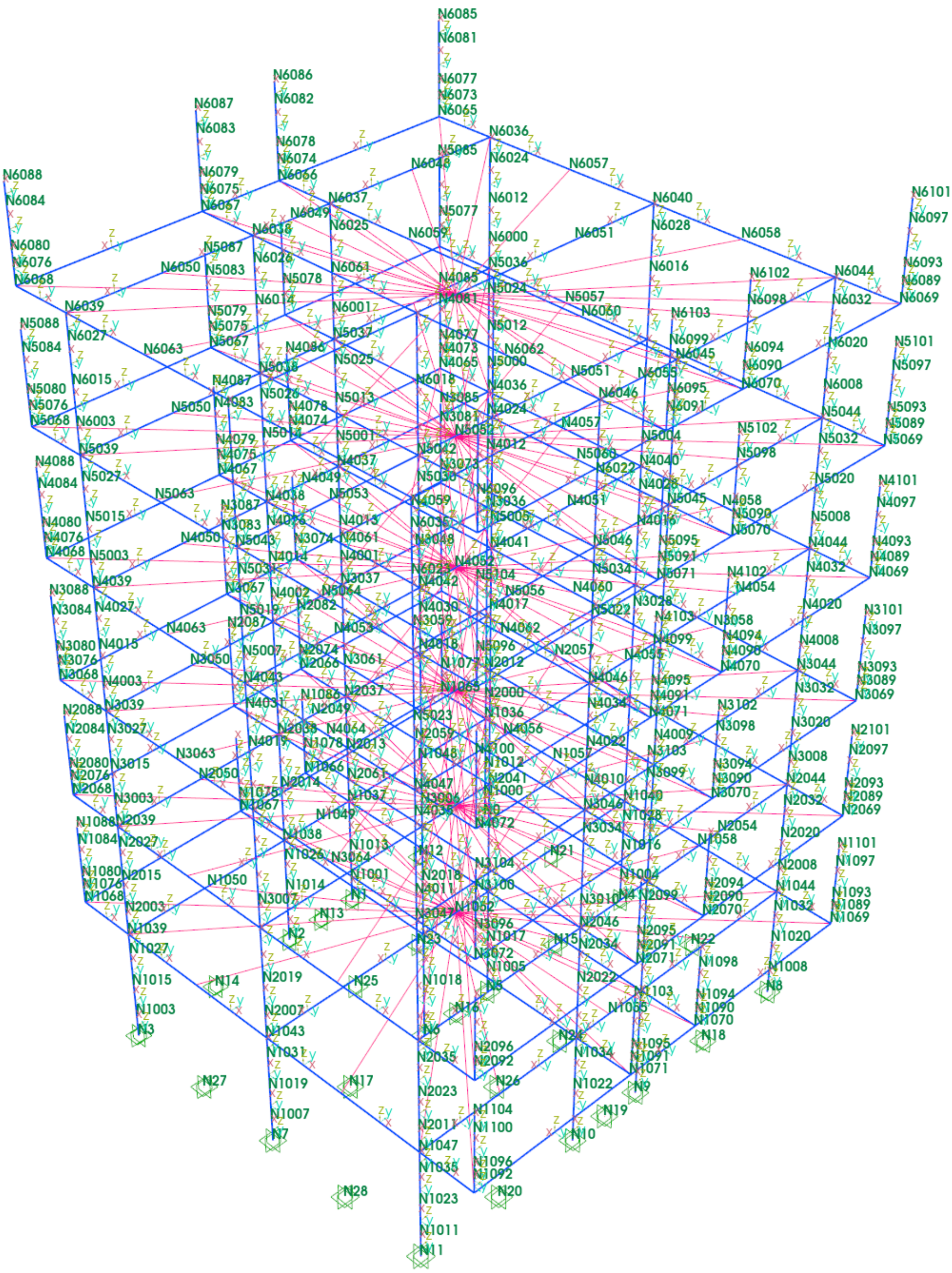

Figure 14 Spatial representation of the Bare frame structure with planters with trees (vertical forest) enabled.

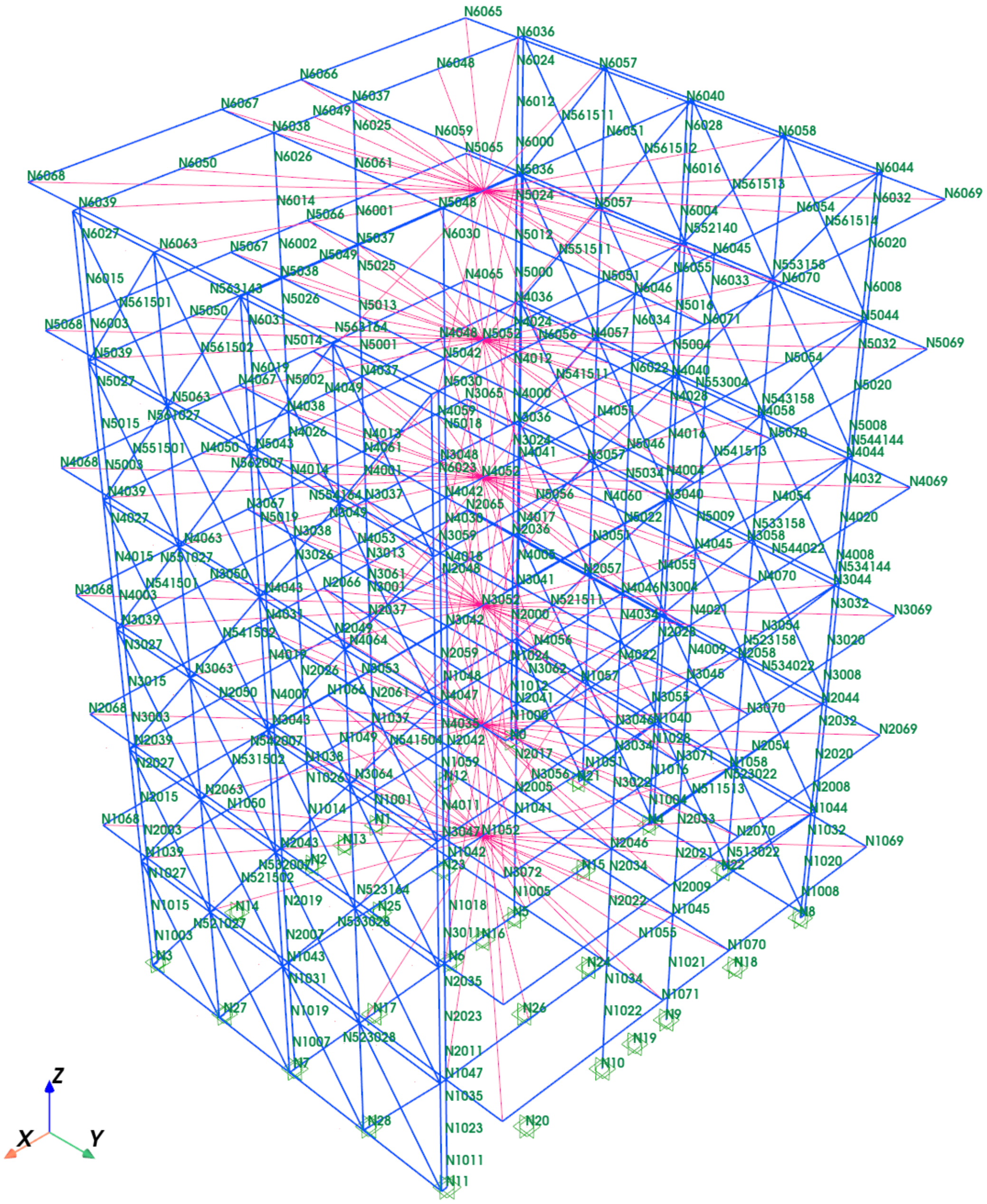

Figure 15 Spatial representation of the Bare frame structure with vertical living walls (vertical forest) enabled.

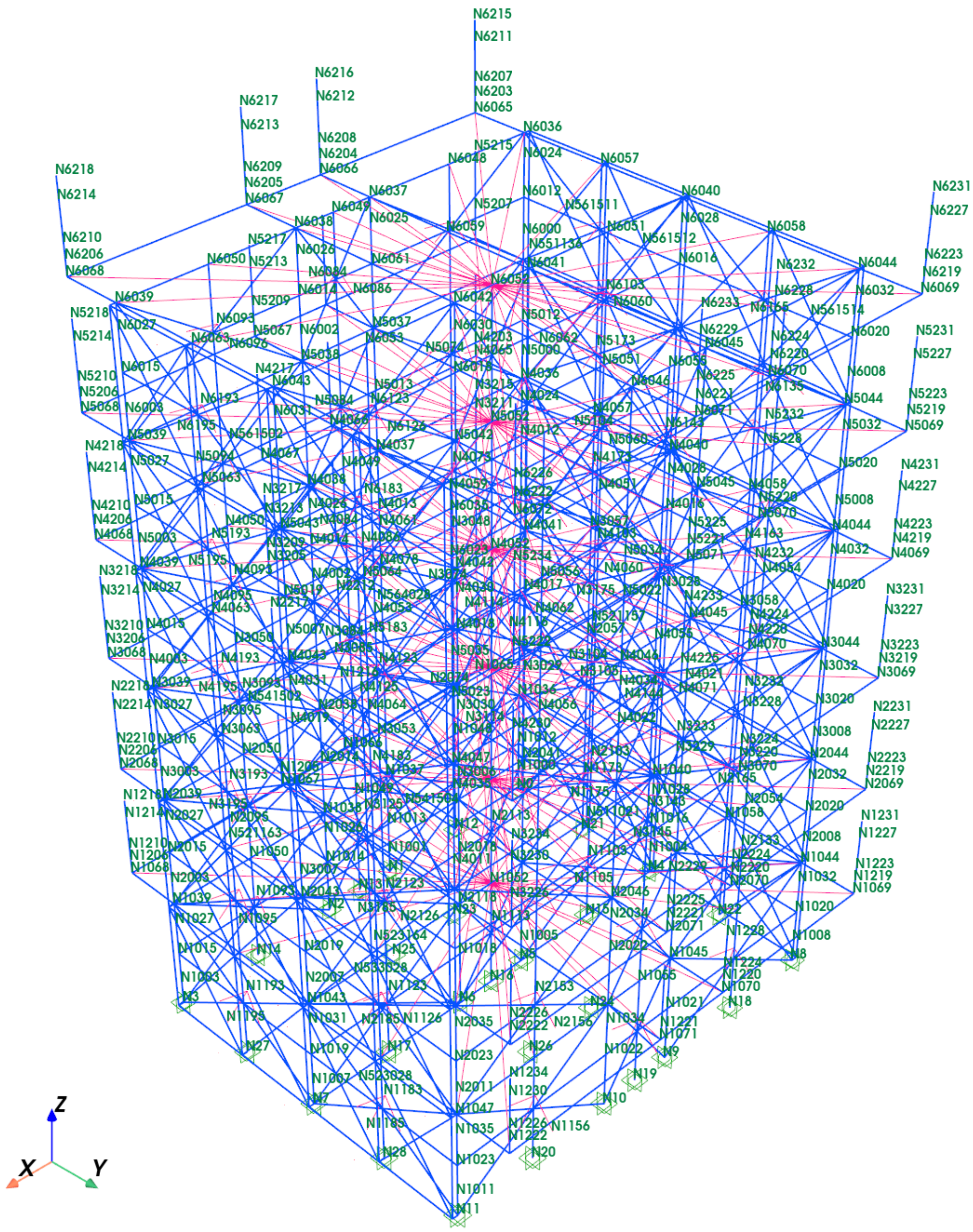

Figure 16 Spatial representation of the Bare frame structure with infills + PUFJ + FRPU + ropes + vertical living walls + planters with trees, vertical forests.

3 MODAL ANALYSIS

For each structural type, a modal analysis was conducted to determine the fundamental dynamic characteristics, specifically the natural periods of vibration and the corresponding mode shapes, which are essential for predicting the seismic response of the structure.

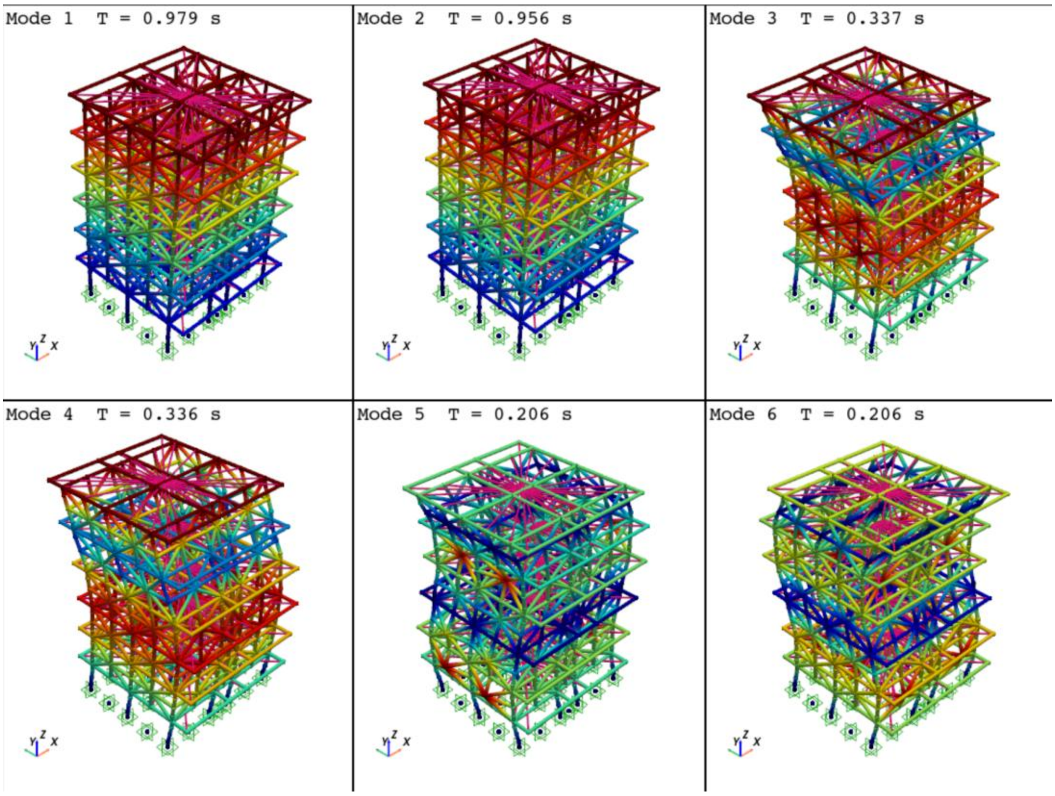

Figure 17 Modes of BFIP.

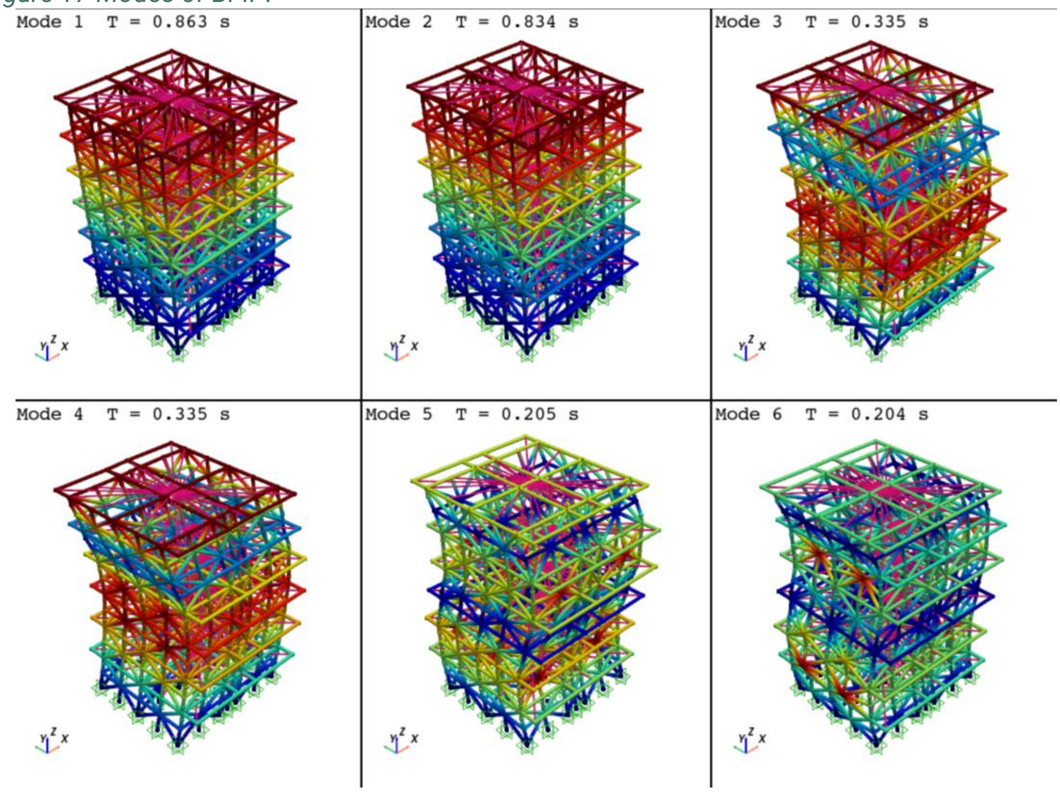

Figure 18 Modes of BFI.

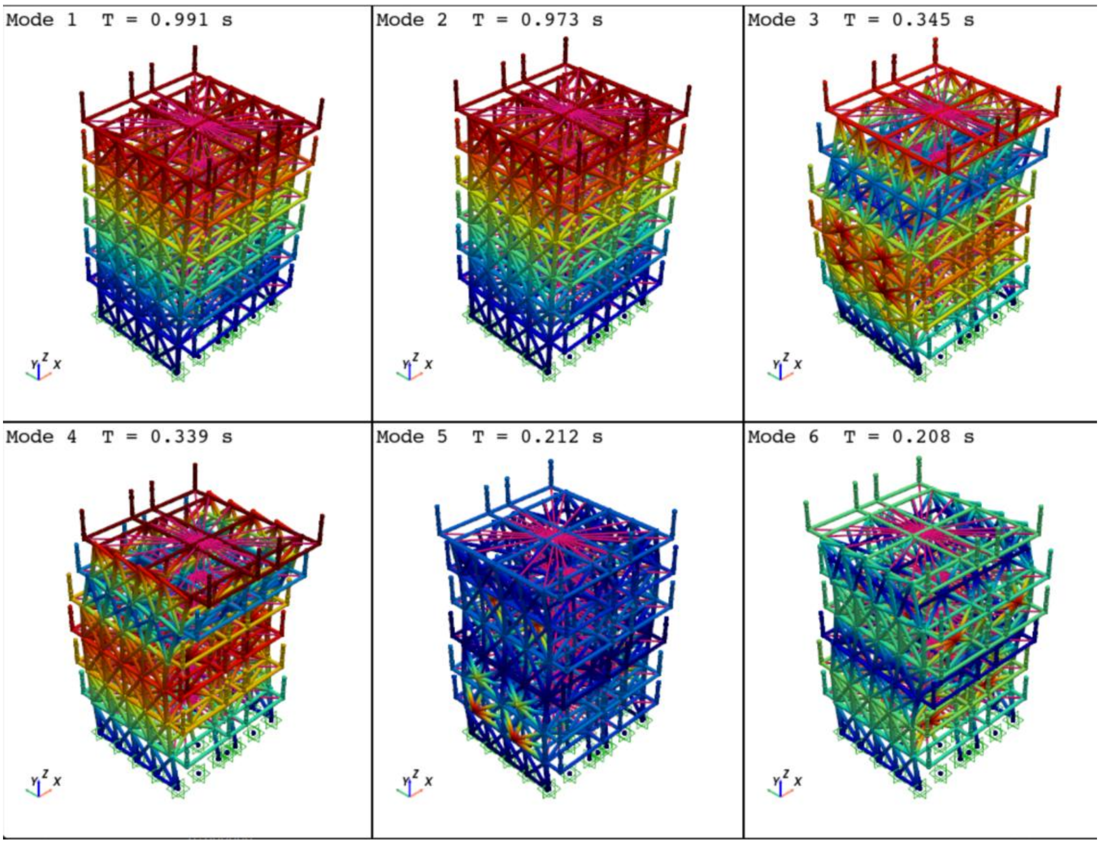

Figure 19 Modes of BFIPR.

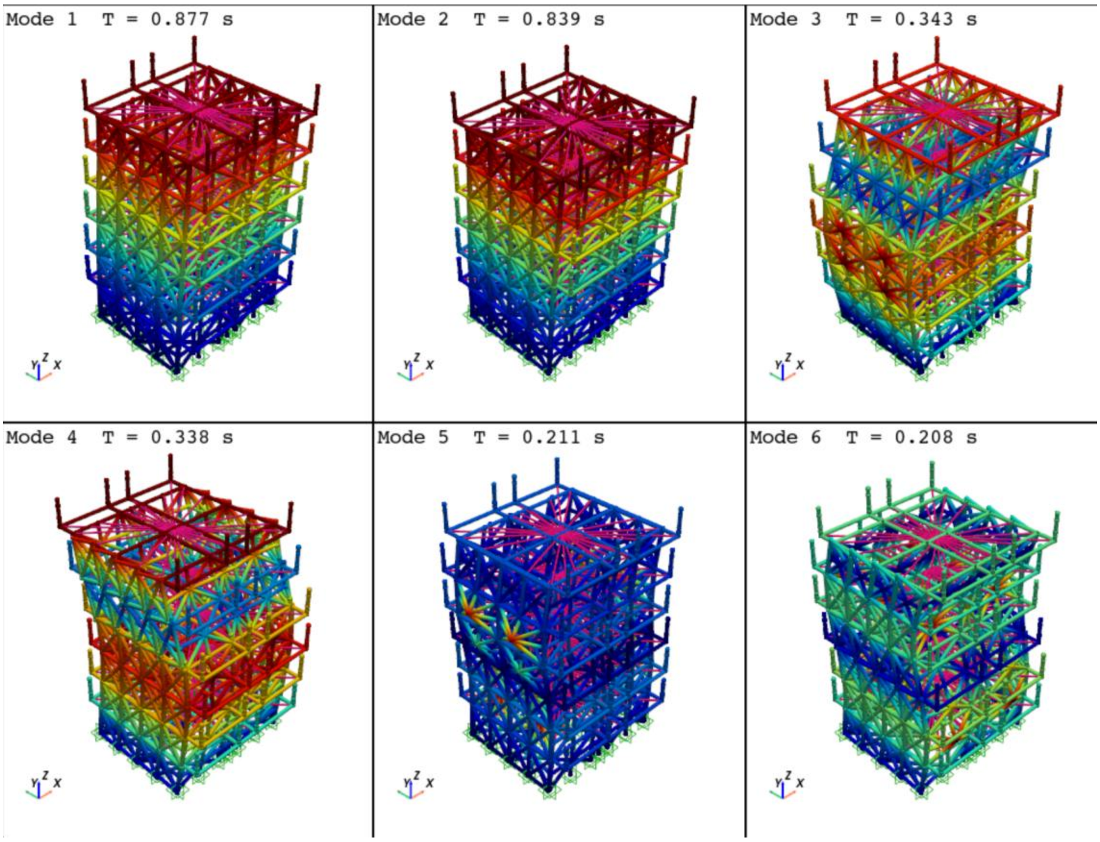

Figure 20 Modes of BFIR.

Table 7 Modes for the RC Structure.

Model	Mode 1	Mode 2	Mode 3	Mode 4	Mode 5	Mode 6	% Cum. mass X	% Cum. mass Y
BFIP	0.979	0.956	0.337	0.336	0.206	0.206	96.7	96.3
BFI	0.863	0.834	0.335	0.335	0.205	0.204	95.9	95.9
BFIPR	0.991	0.973	0.345	0.339	0.212	0.208	95.9	96.1
BFIR	0.877	0.839	0.343	0.338	0.211	0.208	95.2	95.9

BFIP = Bare Frame + Infill + Pilotis, **BFI** = Bare Frame + Infill, **BFIPR** = Bare Frame + Infill + Pilotis + Retrofit , **BFIR** = Bare Frame + Infill + Retrofit

As summarized in Table 7 and illustrated in Figures 17 through 20, the following observations can be made:

- Among the analyzed configurations, the model with full masonry infills (BFI) exhibits the shortest fundamental period (T1=0.863 s), indicating it is the stiffest of the evaluated structures.
- The inclusion of a "pilotis" or soft-story configuration (BFIP) results in a significantly longer fundamental period of 0.979 s compared to the fully infilled model. This increase confirms that the absence of infills at the ground level reduces the floor lateral stiffness, which is a critical factor in seismic vulnerability.
- The retrofitted-strengthened configurations (BFIPR and BFIR) show a marginal increase in natural periods (0.991 s and 0.877 s, respectively) when compared to their non-retrofitted versions.
- Across all models, the first six modes consistently capture over 95% of the cumulative mass in both the X and Y directions. This high level of mass participation confirms that the selected modes provide a sufficiently accurate and comprehensive representation of the buildings' dynamic behavior for subsequent structural analysis.

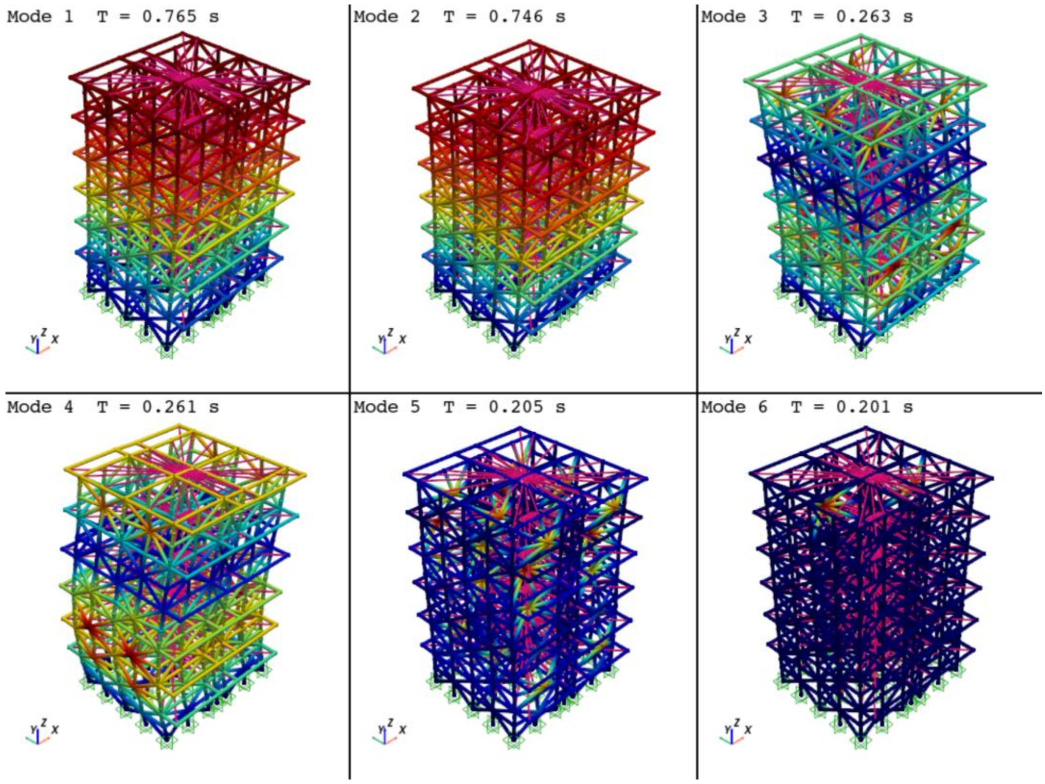

Figure 21 Modes of SBFI.

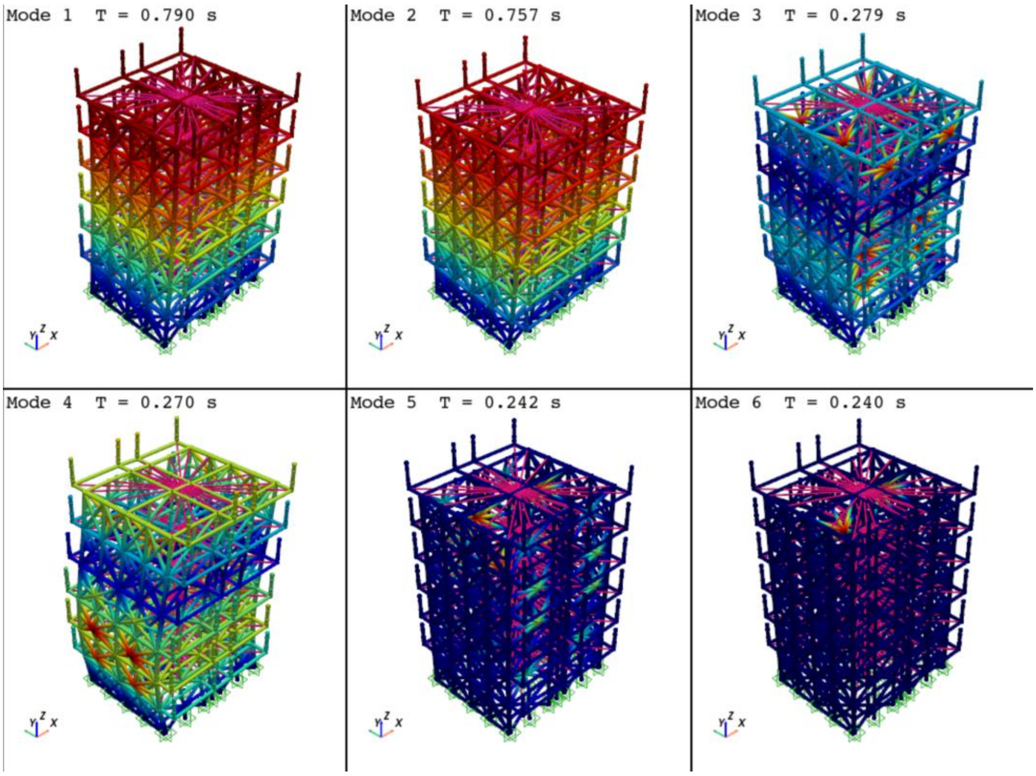

Figure 22 Modes of SBFIR.

Table 8 Modes for the Strong RC Building

Model	Mode 1	Mode 2	Mode 3	Mode 4	Mode 5	Mode 6	% Cum. mass X	% Cum. mass Y
SBFI	0.765	0.746	0.263	0.261	0.205	0.201	93.2	94.4
SBFIR	0.790	0.757	0.279	0.270	0.242	0.240	93.2	93.1

SBFI =Strong: Bare Frame + Infill, Strong: **SBFIR** = Bare Frame + Infill + Retrofit

The modal analysis for the "Strong RC Building" configurations (SBFI and SBFIR) reveals the impact of higher-strength masonry infills on the dynamic characteristics of the structure. The following observations can be made based on the results summarized in Table 8 and illustrated in Figure 21and Figure 22:

- The SBFI model (Strong: Bare Frame + Infill) exhibits a fundamental period (T1) of 0.765 s. When compared to the standard BFI model (T1=0.863 s from Table 7 Modes for the RC Structure.), the SBFI shows a significant reduction in the natural period. This confirms that the use of "strong" infills substantially increases the lateral stiffness of the primary structure.
- Similar to the standard RC building, the retrofitted strong configuration (SBFIR) shows a marginal increase in its natural periods compared to the non-retrofitted SBFI. The fundamental period increases from 0.765 s to 0.790 s. This slight shift suggests that while the retrofit provides strengthening and ductility, it also introduces additional mass or alters the stiffness distribution, leading to a slightly more flexible dynamic response in the elastic range compared to the pure SBFI model.

By comparing these results to the standard RC configurations, it is evident that the "Strong" infill models represent a significantly more rigid structural system, which is expected to influence significantly the base shear capacity and top displacement ductility in the non-linear analysis phase of strengthened existing building scenarios.

4 IMPLEMENTATION OF THE PUSHOVER ANALYSES

Following the modal analysis, a non-linear static pushover analysis was implemented to evaluate the lateral load-resisting capacity and inelastic response of the BFI, BFIP, BFIR, and BFIPR models. For this study, a uniform lateral load distribution was adopted. This uniform loading pattern is particularly useful for identifying potential shear-critical behavior and evaluating the performance of the lower stories, which is essential for the configurations featuring ground-floor pilotis (BFIP and BFIPR). The analysis incrementally increases this lateral load until a target roof displacement is achieved (at the top floor node) or structural failure occurs. The primary objective of this non-linear procedure is to generate the capacity curves (base shear vs. roof displacement). By using a uniform loading profile, the analysis provides a conservative assessment of the building's strength and ductility. This allows for a direct comparison between the retrofitted-strengthened models (BFIR and BFIPR) and their original counterparts, confirming whether the retrofitting successfully enhances the energy dissipation capacity and compensates for the stiffness irregularities caused by the pilotis floor. The results for the pushover analyses for the two existing buildings (with light or heavy brick infill walls) are presented in Figure 23, Figure 24, Figure 25, Figure 26, Figure 27, Figure 28 and the results are compared in the P-d curves depicted in Figure 29.

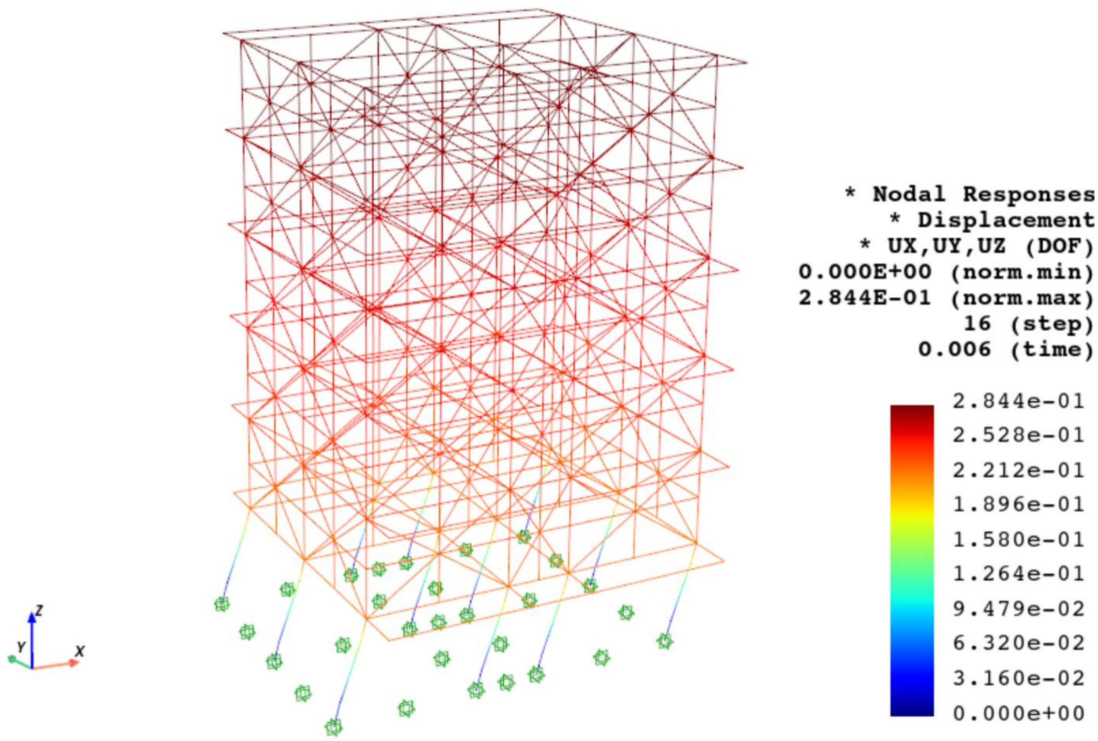

Figure 23 Pushover of BFIP Uniform (units in m).

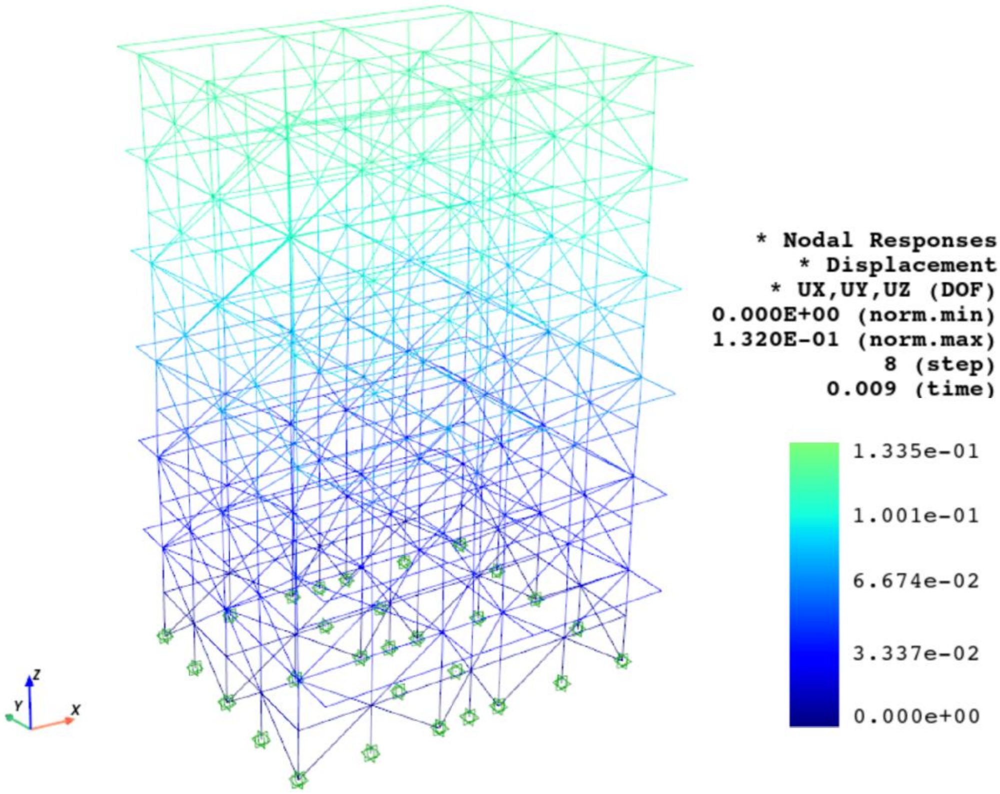

Figure 24 Pushover of BFI Uniform (units in m).

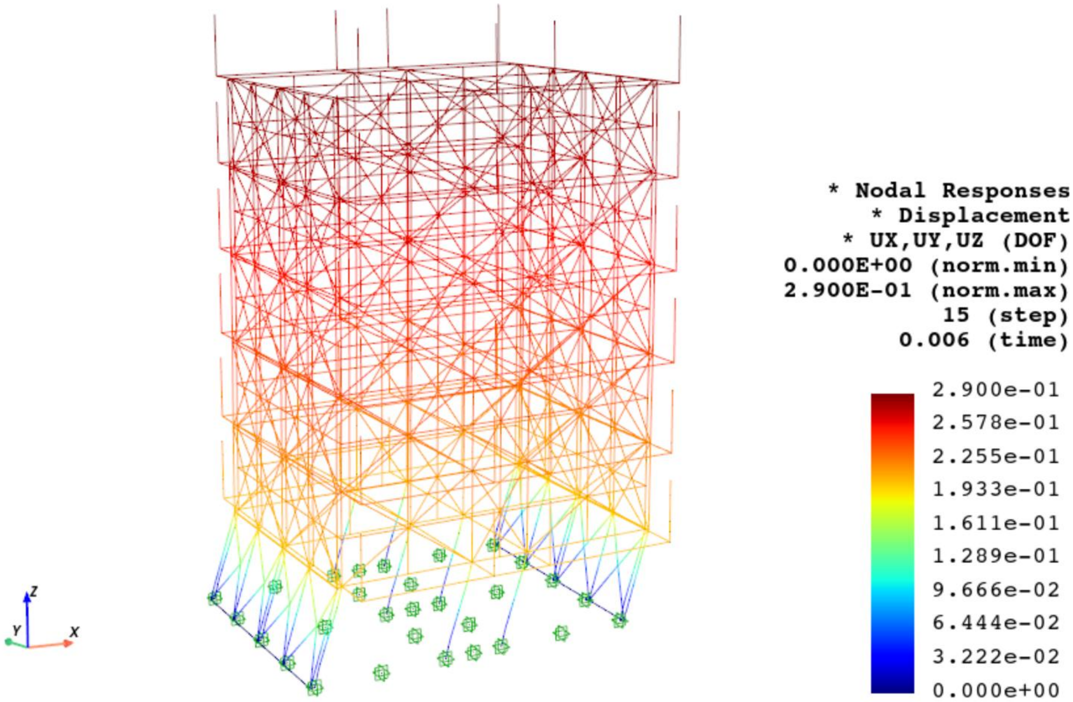

Figure 25 Pushover of BFIPR Uniform (units in m).

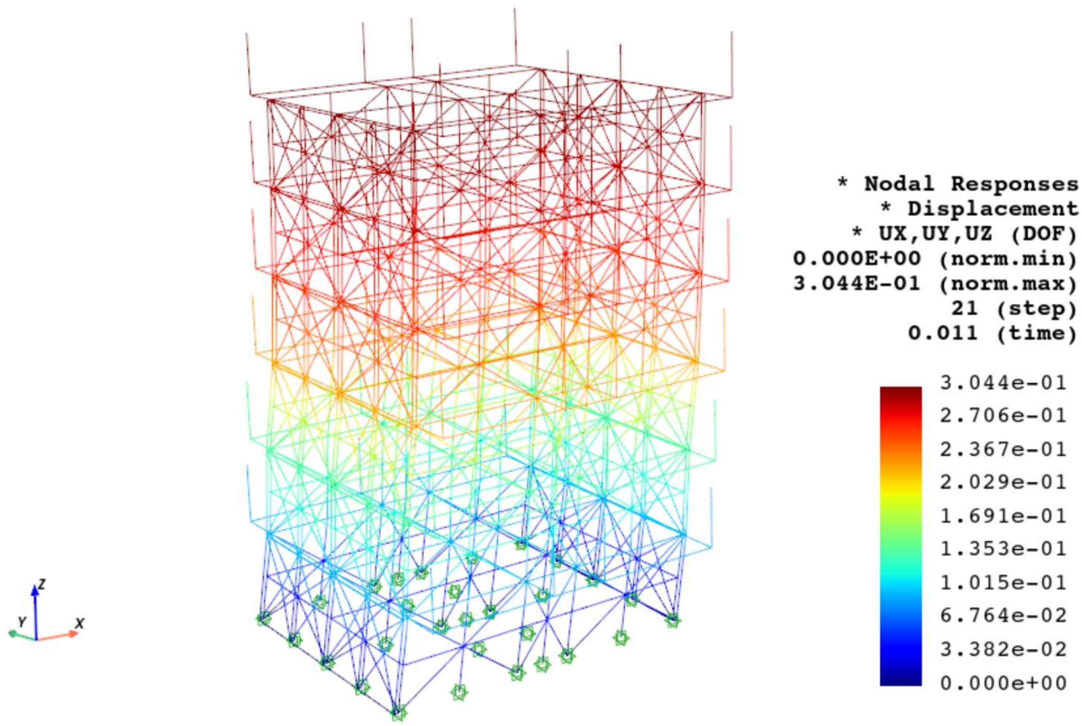

Figure 26 Pushover of BFIR Uniform (units in m).

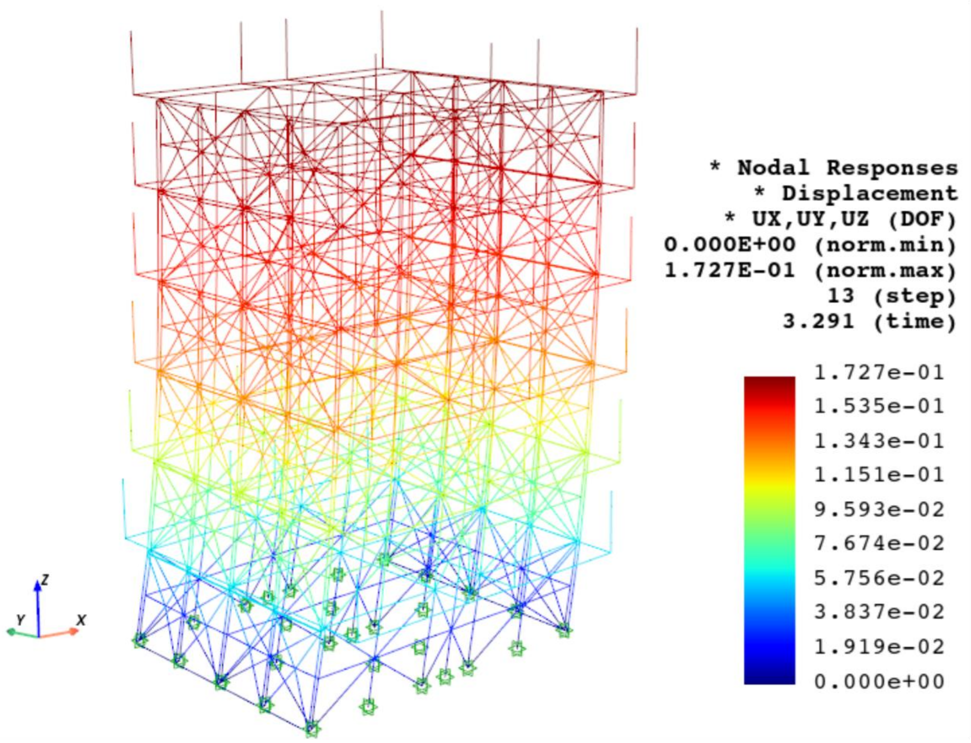

Figure 27 Pushover of SBFIR Uniform (units in m).

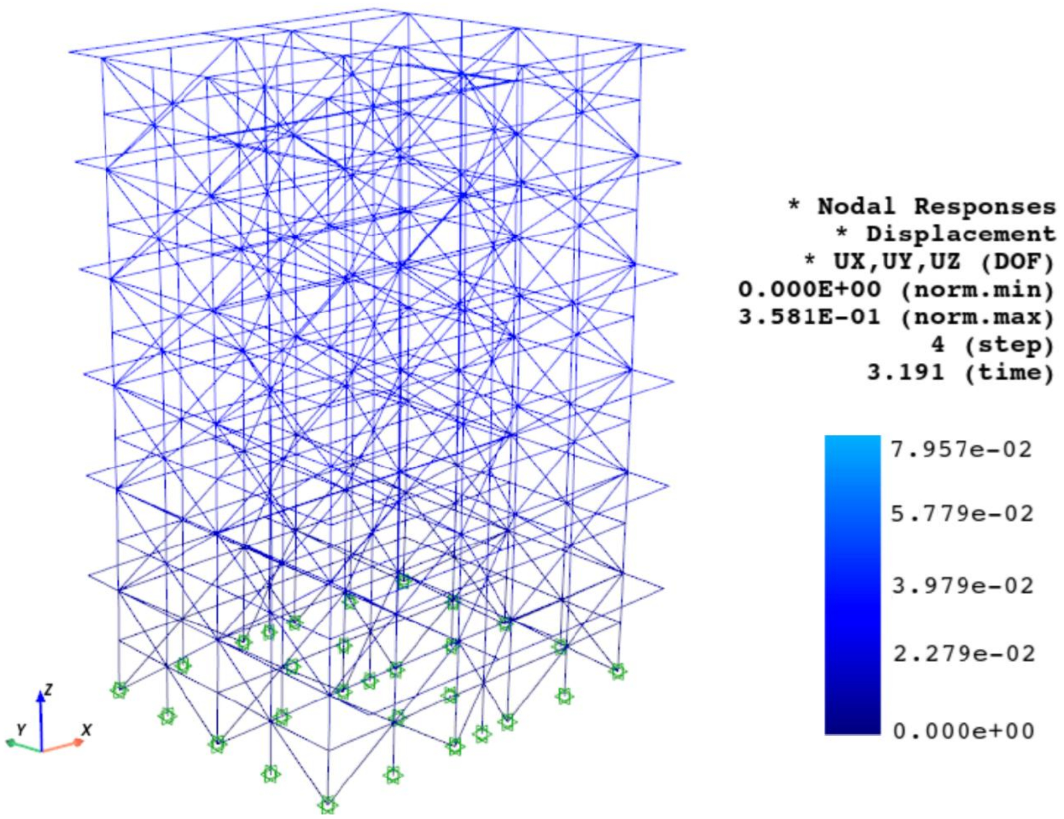

Figure 28 Pushover of SBFI Uniform (units in m).

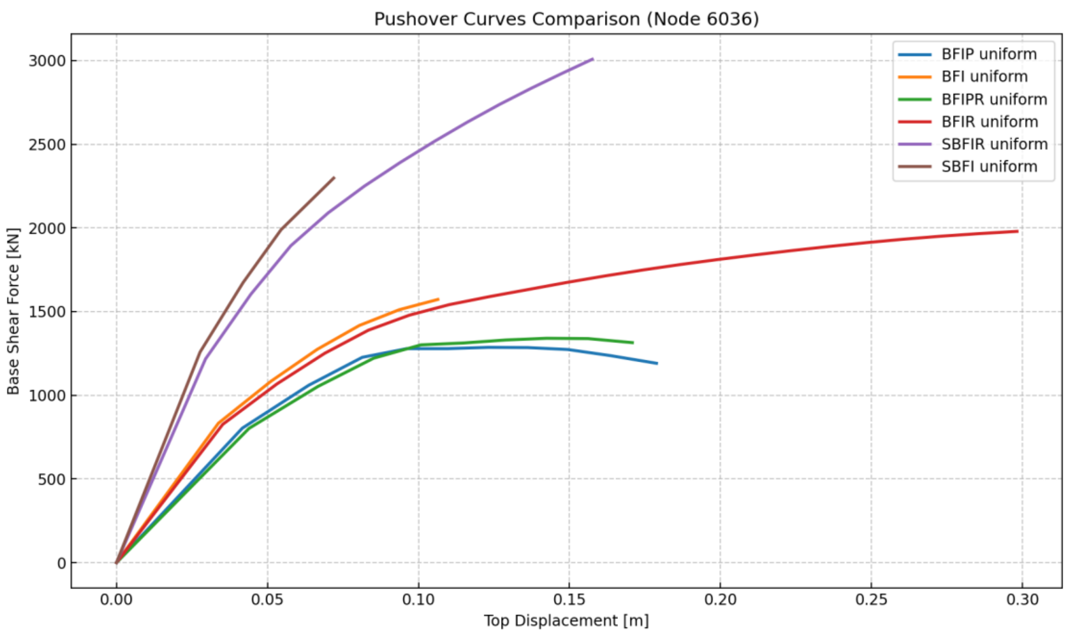

Figure 29 Pushover P-d Curves (Comparative for Uniform horizontal load distribution).

The curves provided in the Figure 29 are terminated in cases when a significant amount of damage is accumulated in any infill configuration. The BFI model (that has infills in all floors) exhibits a higher initial slope compared to the BFIP (Pilotis) models. This confirms that the presence of infills at the ground floor increases the global lateral stiffness. The "S" (Stronger) models, which correspond to the near-field earthquake scenario with quadruple infill thickness, show the highest initial stiffness of all configurations.

The models with a pilotis ground floor (BFIP and BFIPR) reach a significantly lower peak base shear (approx. 1300 kN) compared to the fully infilled BFI counterparts (approx. 1600 kN to 3000 kN). The BFIP uniform curve (Blue) shows a distinct descending branch after 0.15m displacement. This represents the "soft-storey" mechanism where damage concentrates at the ground level, leading to global instability and loss of lateral capacity.

The retrofitted version (BFIR, Red line) not only increases the maximum base shear but, more importantly, provides significant top displacement ductility. While the BFI model terminates at ~0.11m, the BFIR model maintains its capacity up to 0.30m top displacement.

The retrofitting in the pilotis model (BFIPR, Green line) may enable the structure for higher displacement ductility but without altering the undesirable concentration of high column end-rotations at the 1st floor.

The SBFIR (Purple) reaches the highest base shear, among all buildings' cases (~3000 kN). This demonstrates that by combining thick infills with advanced retrofitting that engages the infills through PUFJ and FRPU, the building's base shear capacity is remarkably upgraded. Further, the SBFIR (Purple) version shows much higher top displacement ductility as well. The pushover analyses indicate that the advanced retrofitting-strengthening (ropes/FRPU/PUFJ) enables the building to achive adequate structural integrity despite the addition of vertical forest renovation.

Therefore, the addition of suitable strong brick infill walls in cases of pilotis or other soft storey scenarios, together with advanced seismic joints, surface jackets and rope confinement may lead to desirable overall structural performance of the building by reconfiguring the desirable collapse mechanism while relatively relieving the RC frame.

5 IMPLEMENTATION OF THE DYNAMIC TIME HISTORY IN CASE OF LIGHT INFILLS AND MULTIPLE FAR-FIELD EARTHQUAKE SCENARIO

To analyze the impact of far-field earthquakes, two configurations—BFI and BFIR—were tested, as they were identified as the most critical following the pushover analyses. The 1978 Thessaloniki earthquake was applied to all buildings using dynamic pushover analysis approach, consistent with the methodology in (Rousakis et al., 2024). The load intensity was scaled to peak ground accelerations (PGA) of 0.1g, 0.2g, and 0.5g. The primary objective was to investigate the impact of the additional infrastructure and mass from the greenery and the various interventions on the response of the existing building considering an SLS level, moderate earthquake excitation scenario.

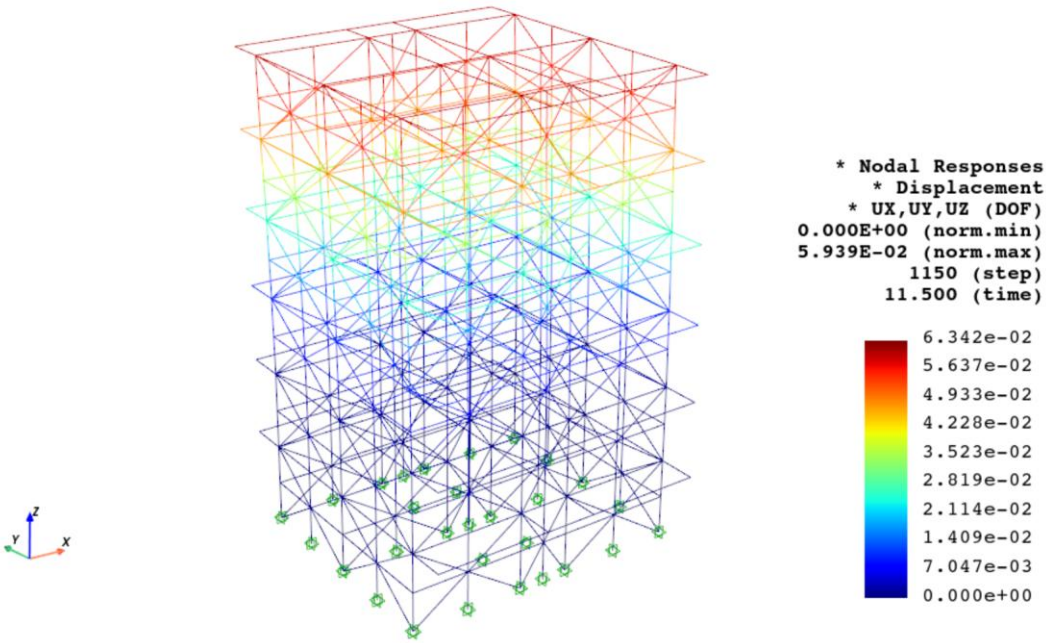

Figure 30 Dynamic analysis results for BFI: Maximum nodal displacement (units in m) under 0.5g PGA.

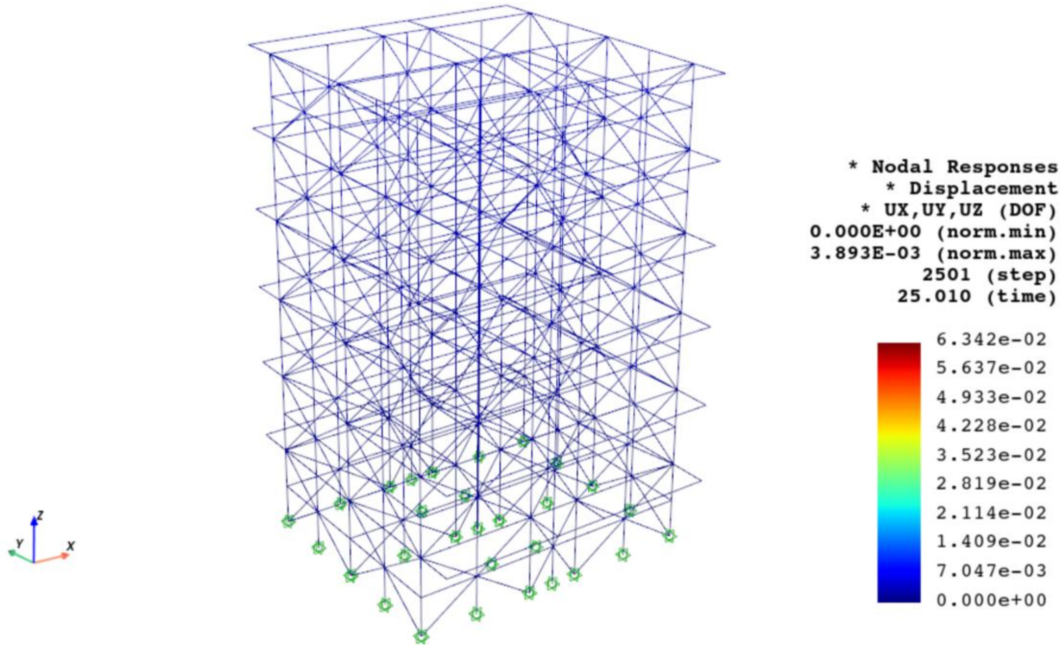

Figure 31 Dynamic analysis results for BFI: Deformed shape at the end of simulation (units in m) under 0.5g PGA.

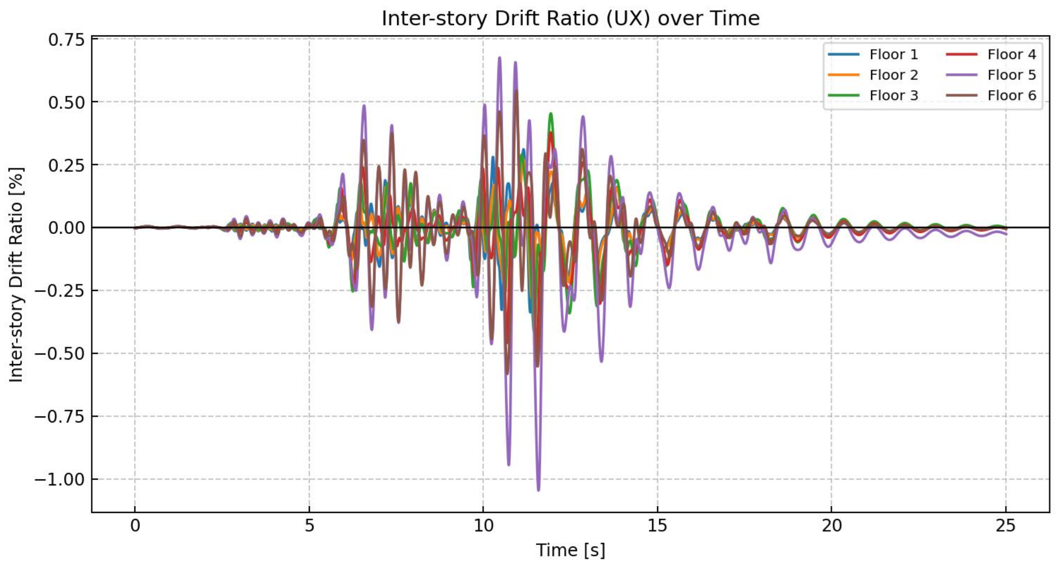

Figure 32 Dynamic analysis result for BFI: IDR time history results for all floors under 0.5g PGA.

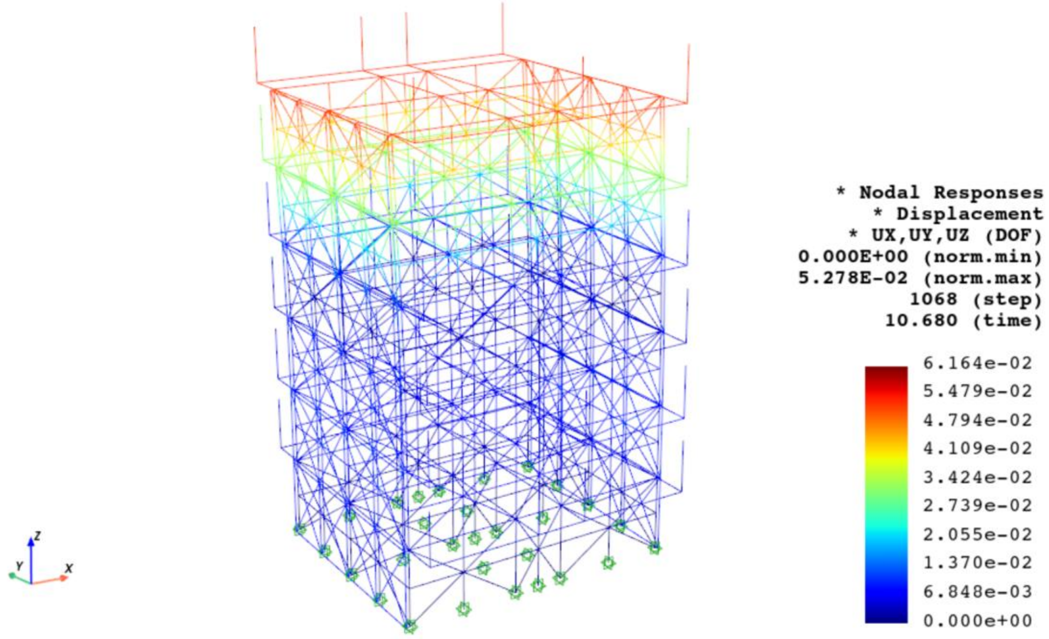

Figure 33 Dynamic analysis results for BFIR: Maximum nodal displacement (units in m) under 0.5g PGA.

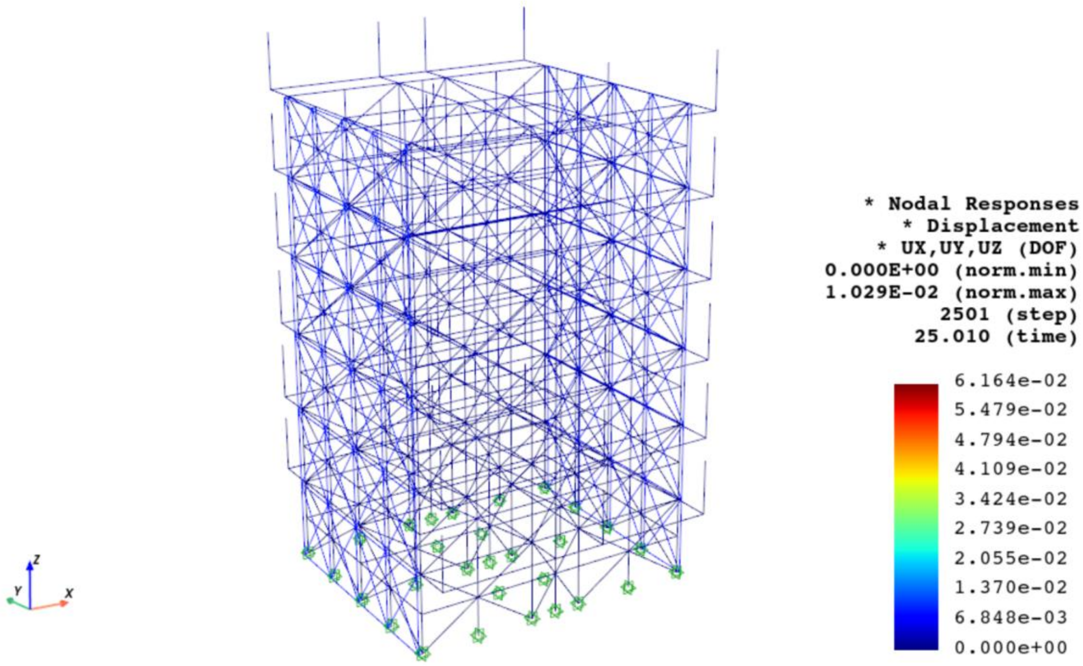

Figure 34 Dynamic analysis results for BFIR: Deformed shape at the end of simulation (units in m) under 0.5g PGA.

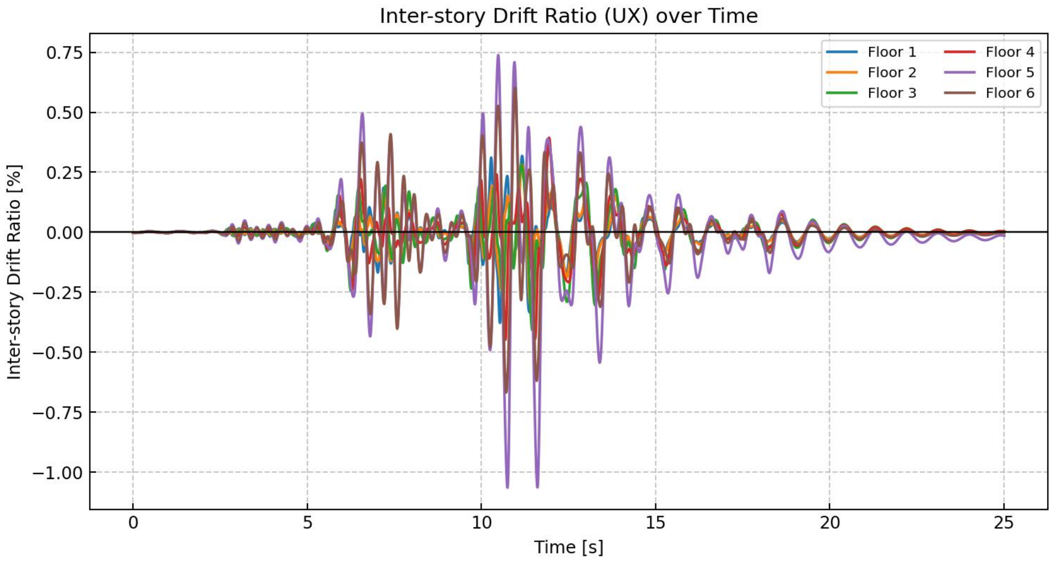

Figure 35 Dynamic analysis result for BFIR: IDR time history results for all floors under 0.5g PGA.

Figure 30 and Figure 31 illustrate the global displacement field of the BFI model at the point of maximum drift and at the conclusion of the 0.5g far-field earthquake. The Inter-story Drift Ratio (IDR) time history for all floors (Figure 32) indicates that the bare frame with infills undergoes significant oscillations, with peak drifts occurring primarily in the middle stories. By comparison, the retrofitted BFIR model (Figure 33, Figure 34, Figure 35) demonstrates a more controlled response despite the increased mass (and the infrastructure) of the vertical forest renovations. The IDR results for BFIR show that the interventions successfully keep peak drift values and distributed the seismic demand more uniformly across the building height, preventing local story mechanisms. Primarily, the last 2 floors exhibit significant drift ratios, but around to 1% only.

6 IMPLEMENTATION OF THE DYNAMIC TIME HISTORY IN CASE OF HEAVY INFILLS AND NEAR-FIELD EARTHQUAKE SCENARIO

A near-field seismic scenario, utilizing the 1995 Kobe earthquake record scaled to 40% of peak acceleration magnitude, was tested for two critical configurations: the reinforced concrete frame with infills on all floors (SBFI) and its retrofitted-strengthened counterpart (SBFIR). The retrofitting strategy for SBFIR included 35 mm seismic joints between the columns and the infills, confinement ropes in the critical regions of the columns, and FRPU mesh on the surface of the infills. It has been established (Rousakis et al., 2020) that a 20 mm thick PUFJ seismic joint (that is 1% of brick infill height) can prevent significant damage accumulation in masonry infills up to a 2.5% RC column drift ratio. In contrast, standard infills without seismic joints typically accumulate significant damage at drift ratios between 0.5% and 1.0%. The simulations were configured to terminate once significant damage was anticipated. For the unreinforced building (SBFI), the simulation was terminated when the maximum drift ratio reached around 0.5%. In that time step the in-plane infills of the first three floors surpassed this threshold. For the retrofitted building (SBFIR), the infills sustained peak drifts as high as around 2.5% at the base floor, while five out of the six floors had drifts higher than 0.5%. Negligible residual top displacement is recorded. The results of the analysis at maximum drift and at the end of the time history are depicted in Figure 36, Figure 38 and Figure 39 while the drift time histories for all floors are shown in Figure 37 and Figure 40.

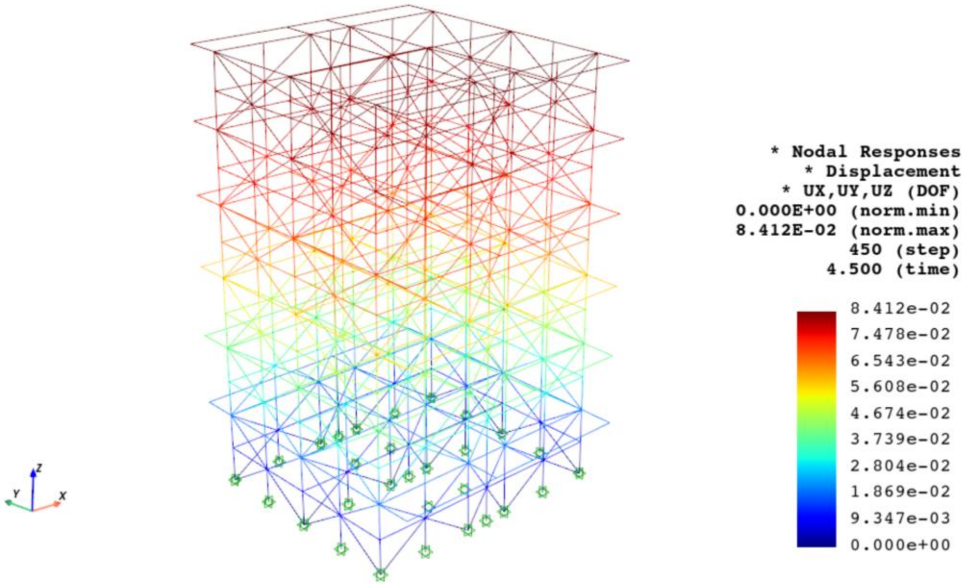

Figure 36 Near-field earthquake analysis result for SBFI maximum drift (units in m).

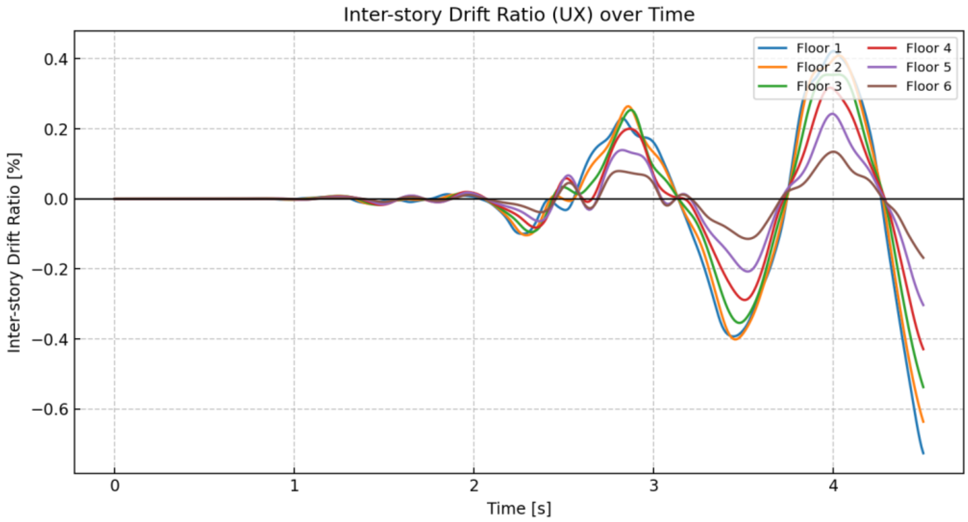

Figure 37 Near-field earthquake analysis result for SBFI: IDR time history results for all floors.

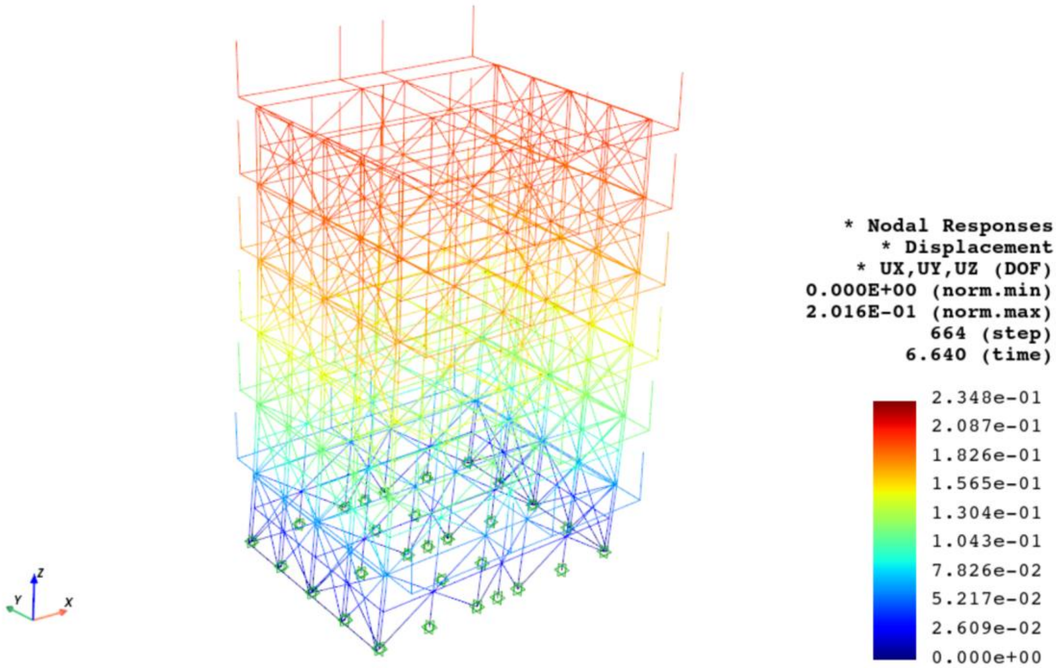

Figure 38 Near-field earthquake analysis result for SBFIR maximum drift (units in m)

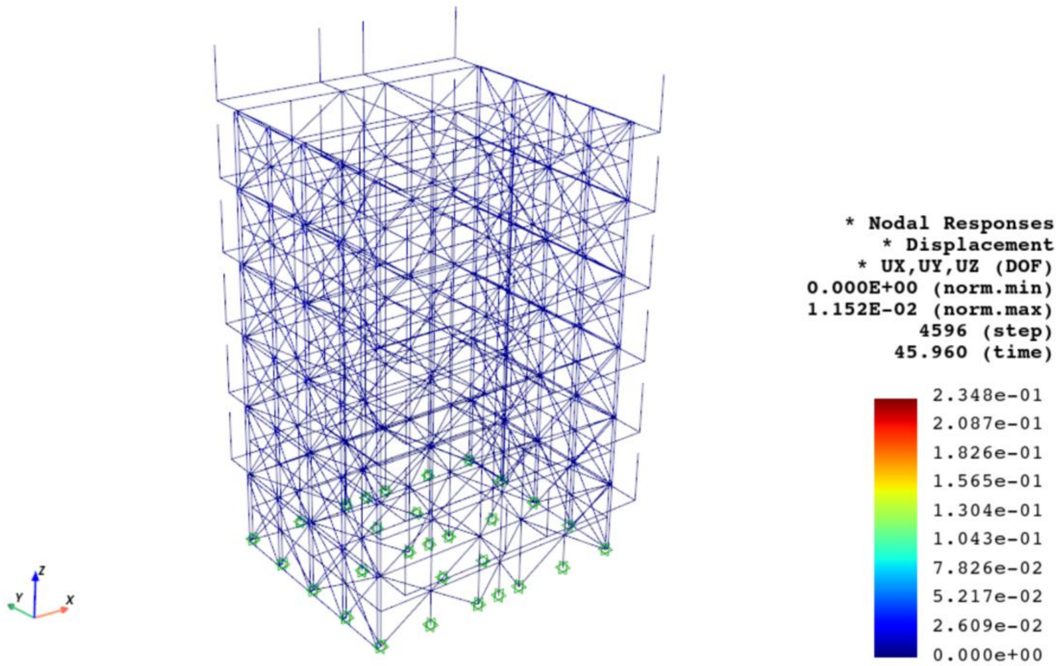

Figure 39 Near-field earthquake result for SBFIR at the end of simulation (units in m)

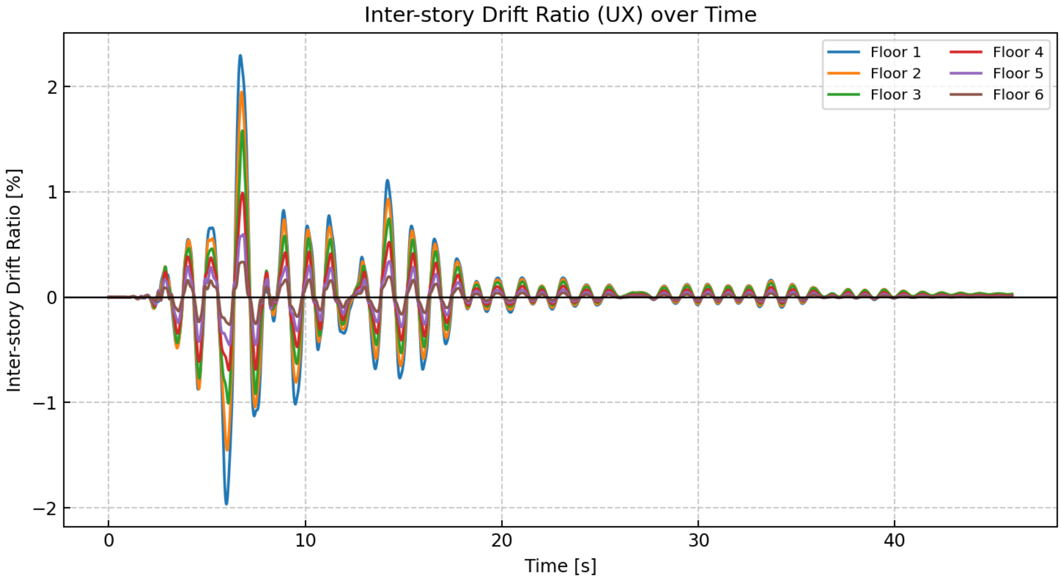

Figure 40 Near-field earthquake result for SBFIR: IDR time history results for all floors.

The near-field earthquake simulation (Kobe 1995) presents a more aggressive seismic demand due to its impulsive nature. As shown in Figure 37, the SBFI model reached the termination criterion of 0.5% drift within the first 4 seconds of the simulation, indicating a high risk of collapse for the infill walls without innovative interventions (first three floors). Conversely, the strengthened (retrofitted with basalt ropes + PUFJ + FRPU) SBFIR model (Figure 38, Figure 39, Figure 40) managed to sustain the full duration of the record. Although the IDR values reached higher peaks (surpassing 2%) compared to the far-field case, the structure maintained its stability, confirming the effectiveness of the PUFJ and seismic joints in accommodating the large displacements characteristic of near-field ground motions.

7 VERTICAL FOREST PLANTER FREE END AND VERTICAL LIVING WALL MIDDLE DISPLACEMENTS

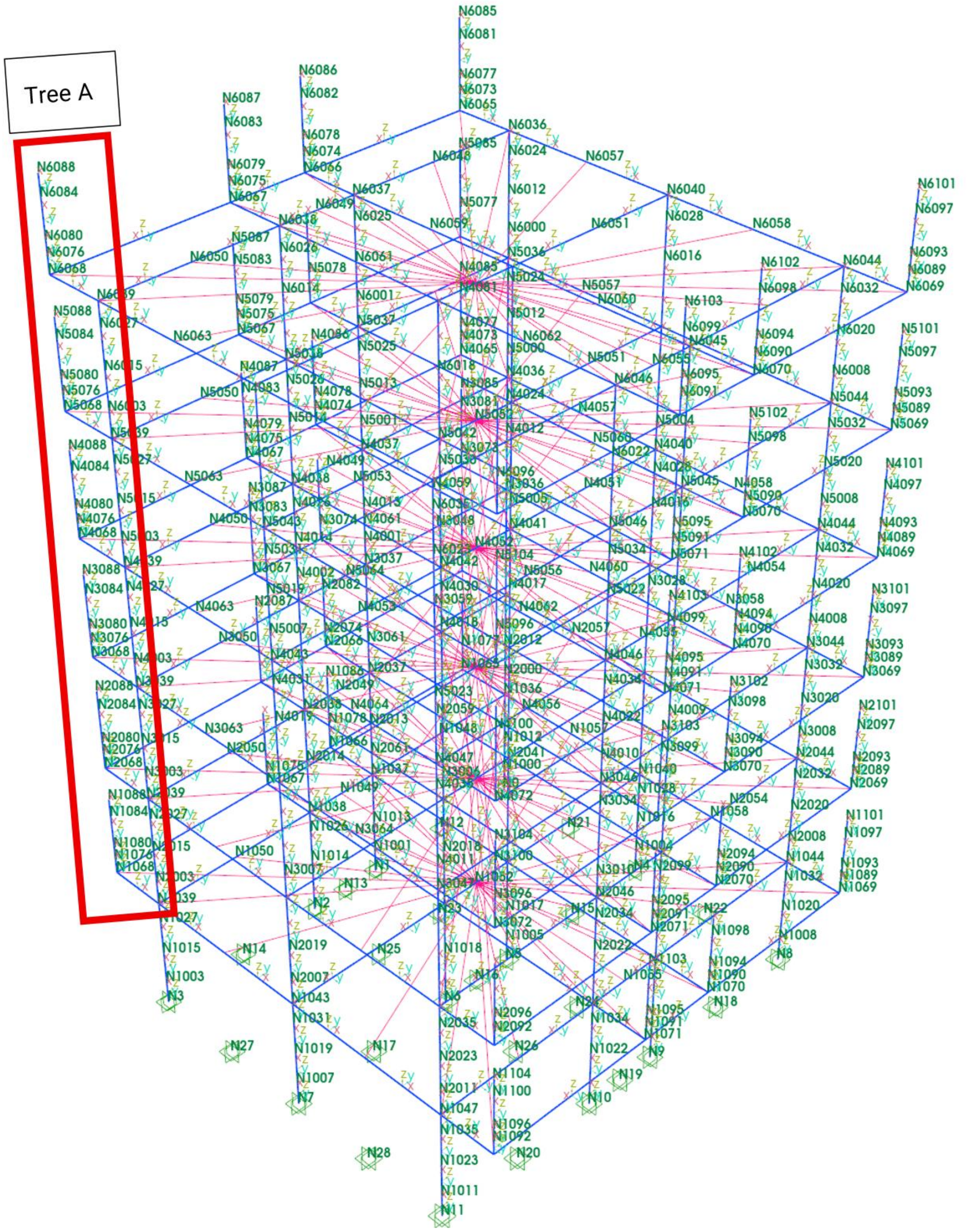

Figure 41 Spatial representation of the Bare frame structure with vertical forest planter enabled and inside the red rectangle is denoted the trees that are monitored during the total seismic excitation.

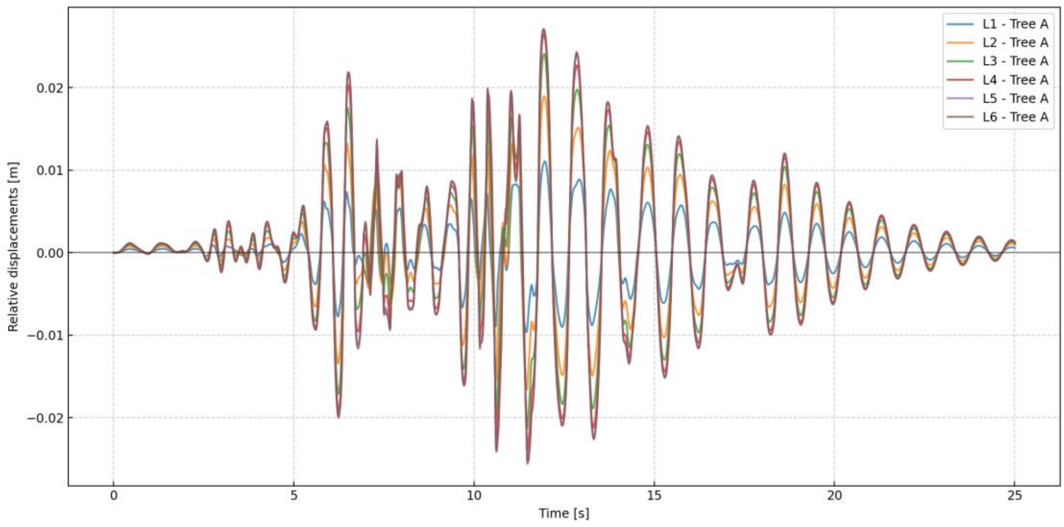

Figure 42 Dynamic analysis result for BFIR: Relative Displacement time history results for all Tree A.

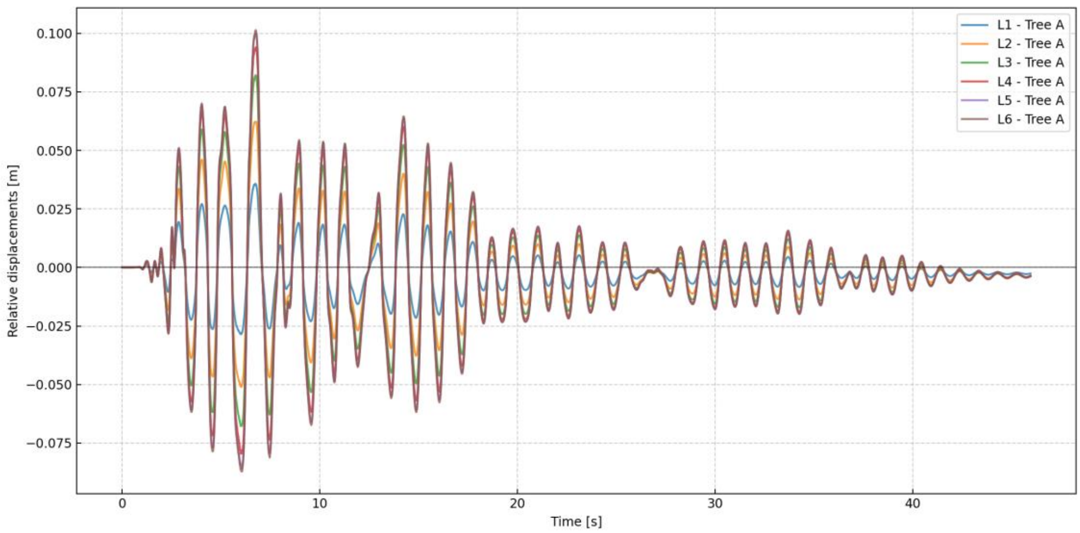

Figure 43 Dynamic analysis result for SBFIR: Relative Displacement time history results for all Tree A.

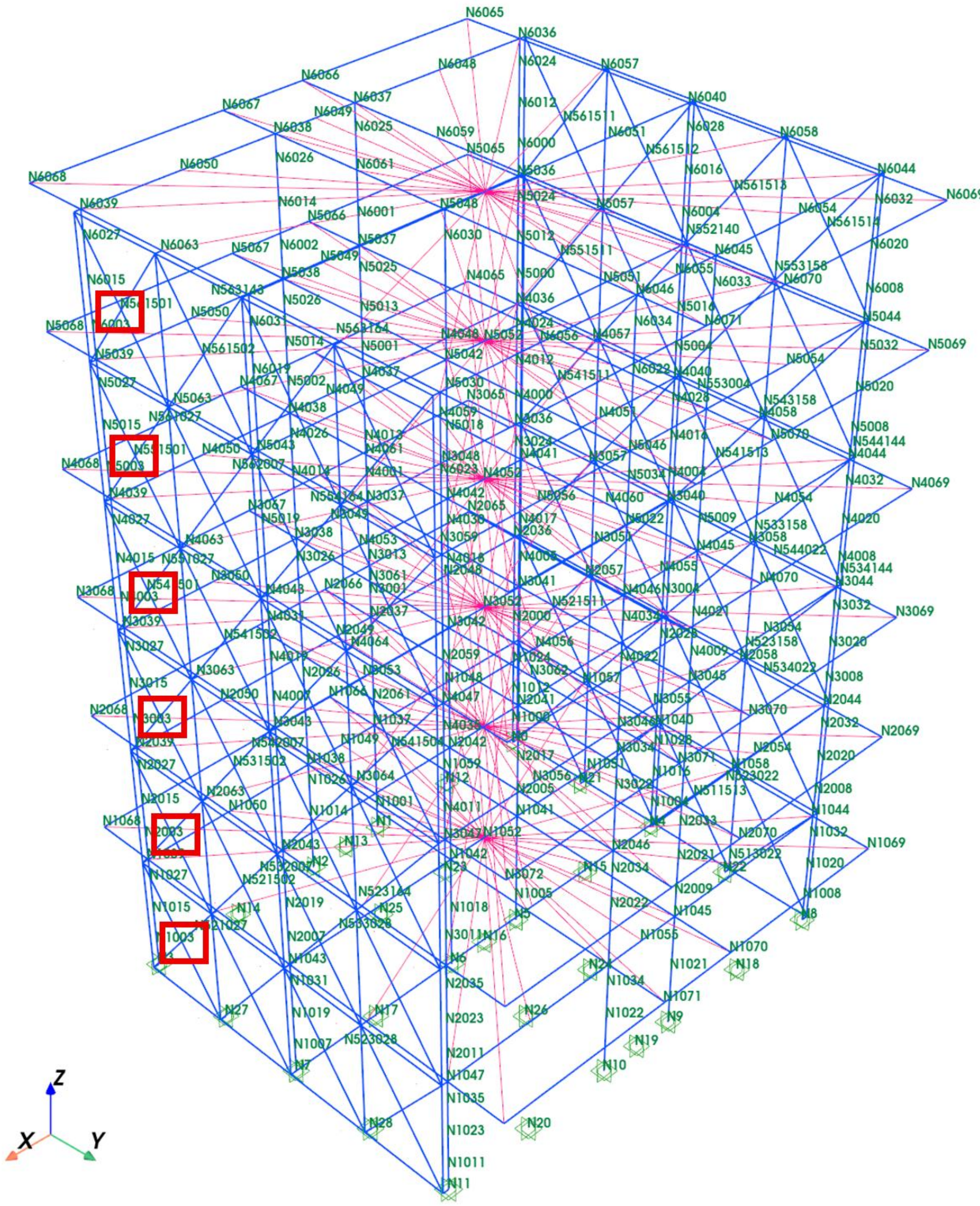

Figure 44 Spatial representation of the Bare frame structure with living walls enabled and inside the red rectangle is denoted the with vertical living walls (LW A) that are monitored during the total seismic excitation.

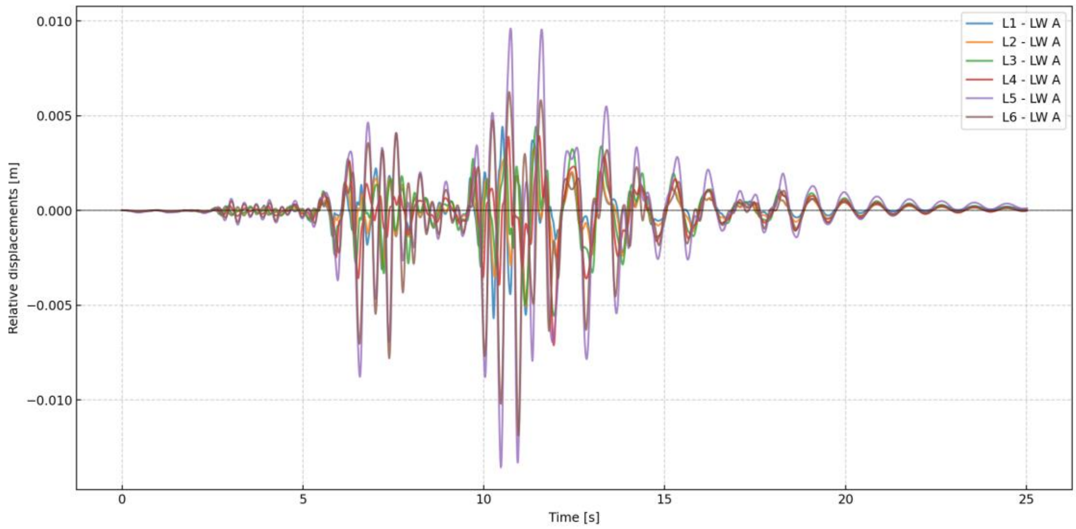

Figure 45 Dynamic analysis result for BFIR: Relative Displacement of Out of Plane time history results for all LW A.

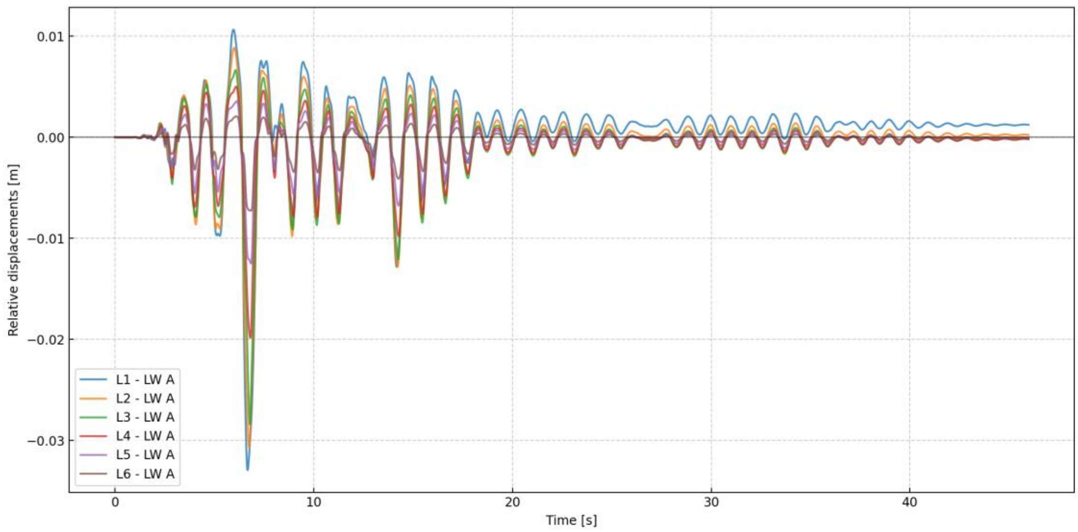

Figure 46 Dynamic analysis result for SBFIR: Relative Displacement of Out of Plane time history results for all LW A.

The monitoring of secondary structural components—specifically the Vertical Forest (Tree A) and Living Walls (LW A)—is essential to evaluate the interaction between the green additions and the RC frame. By analyzing the relative displacement time histories, we can assess the risk of collision (pounding) and the demand on mechanical connections.

The trees, which stand 2.2m tall, are positioned on balconies 1.5m away from the building envelope. As shown in the dynamic analysis for the SBFI model (Figure 43), the peak relative displacement for the trees under 0.3g excitation reaches approximately 0.10m (10cm). Besides, there is a relatively more intense oscillation of the trees all over the time history with respect to the buildings' damping. As the horizontal distance to the building envelope is 1.5m, a relative displacement of 0.10m represents only 6.7% of the available clearance. This confirms there is no risk of the trees striking the building facade during a 0.3g severe seismic event X and in Y direction (as the structure is almost symmetric).

The Vertical Living Walls are installed with a 15cm (0.15m) horizontal gap from the masonry infills. The monitoring of the Out-of-Plane (OOP) displacement is critical to prevent pounding between the modular green system and the wall. In the most demanding case (SBFIR,

Figure 46), the peak relative displacement of the Living Wall is approximately 0.033m (3.3cm). The plots reveal a distinct phase-lag between the primary structure and the green components. This indicates that the greenery does not move in perfect synchronization with the RC frame, which creates inertial forces on the mounting brackets. However, because the relative displacements are limited to 3.3cm for the Living Walls and 10cm for the trees, the strain on the anchors is significantly lower than the failure threshold of standard steel chemical anchors used in reinforced concrete, ensuring the 'Greenery' interventions are seismically resilient.

8 INFILL WALL MIDDLE DISPLACEMENTS

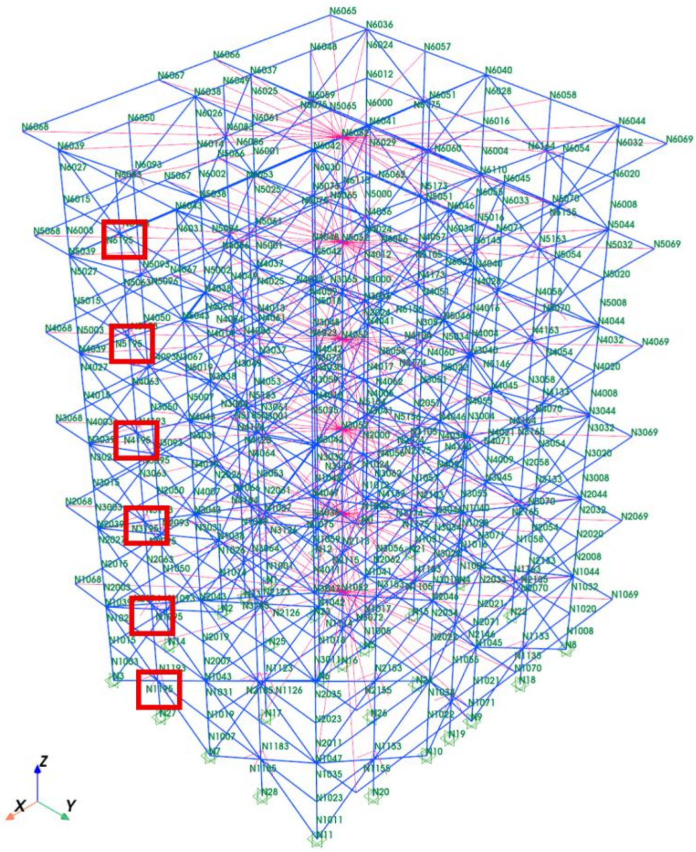

Figure 47 Spatial representation of the Bare frame structure with infills enabled (BFI) and inside the red rectangle is denoted the infill nodes (INFILL A) that are monitored during the whole seismic excitation (0.5g).

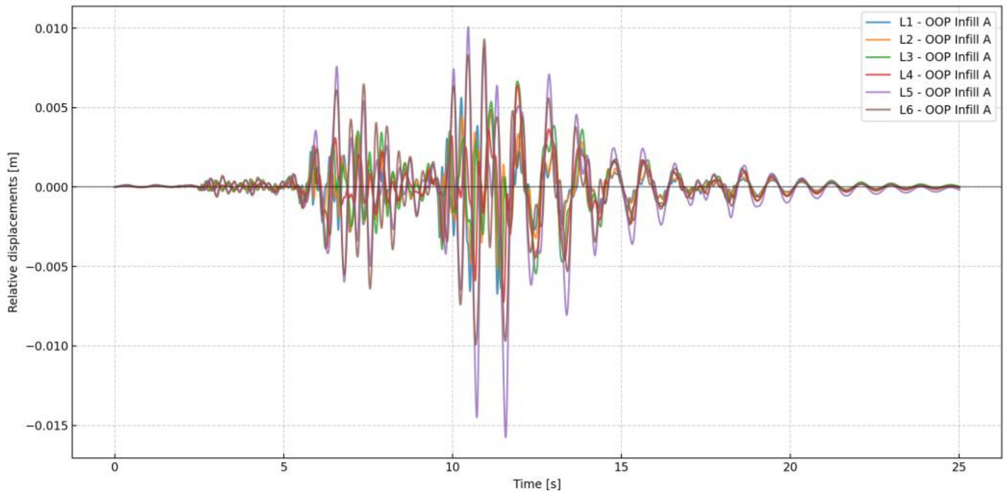

Figure 48 Dynamic analysis result for BFI: Relative Out-of-Plane displacement time history results for all INFILL A middle point (0.5g).

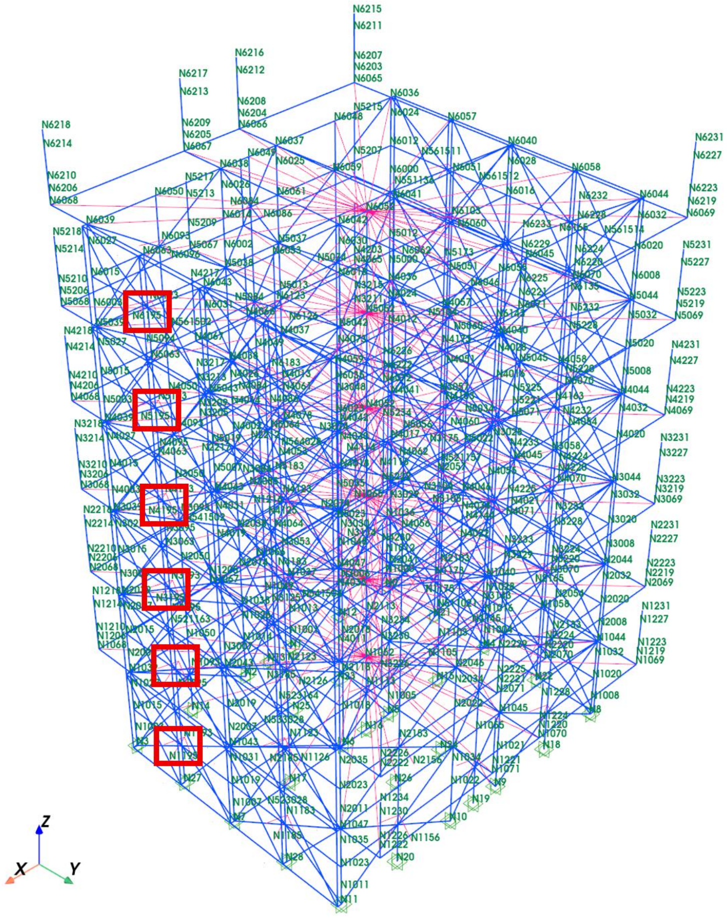

Figure 49 Spatial representation of the Bare frame structure with infills enabled (BFIR) and inside the red rectangle is denoted the infill nodes (INFILL A) that are monitored during the total seismic excitation (0.5g).

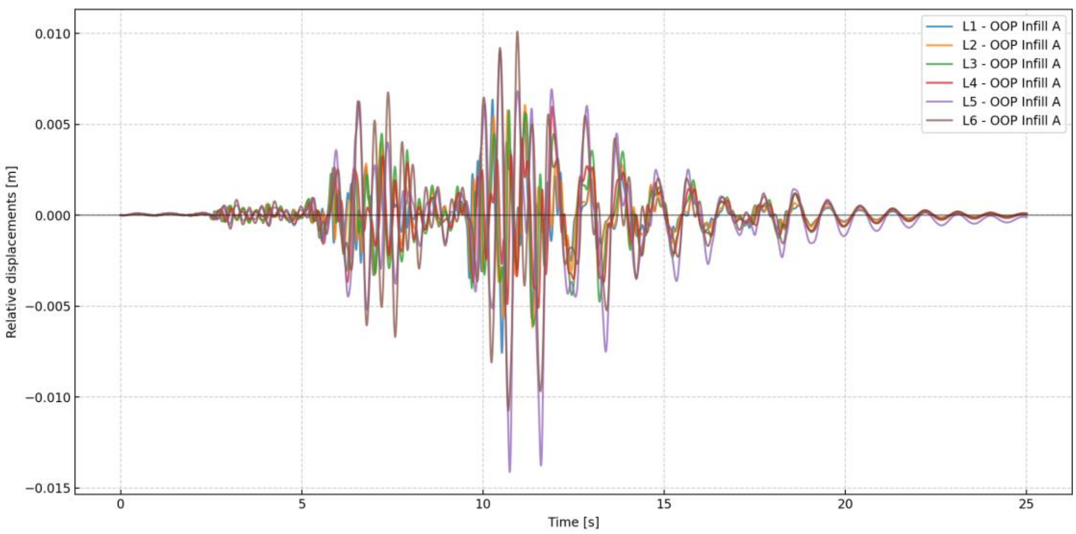

Figure 50 Dynamic analysis result for BFIR: Relative displacement time history results for all INFILL A (0.5g).

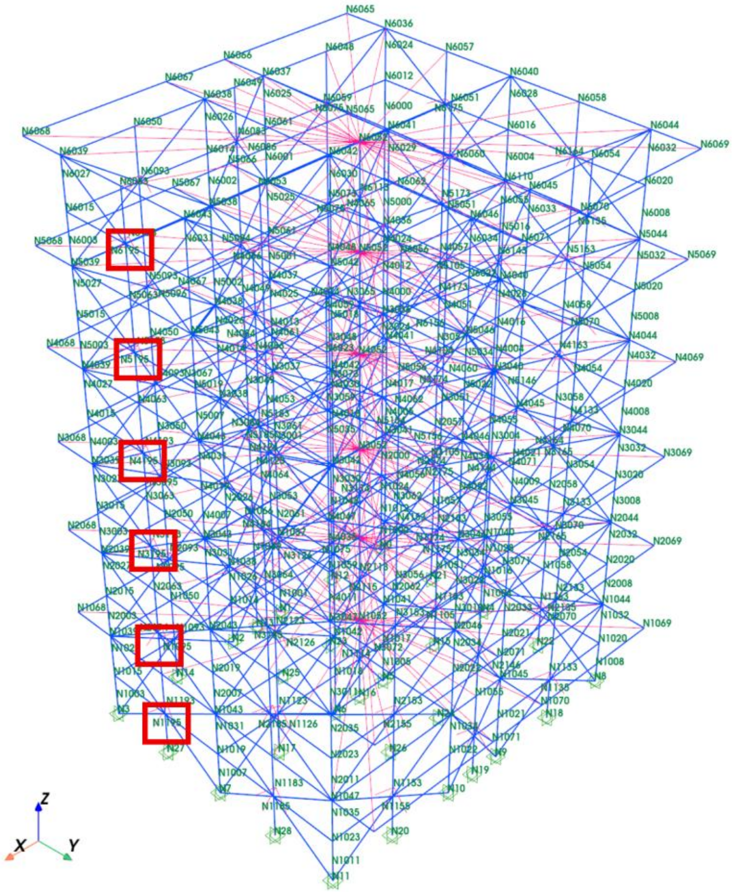

Figure 51 Spatial representation of the Strong Bare frame structure with infills enabled (SBFI) and inside the red rectangle is denoted the infill nodes (INFILL A) that are monitored during the total seismic excitation (0.3g).

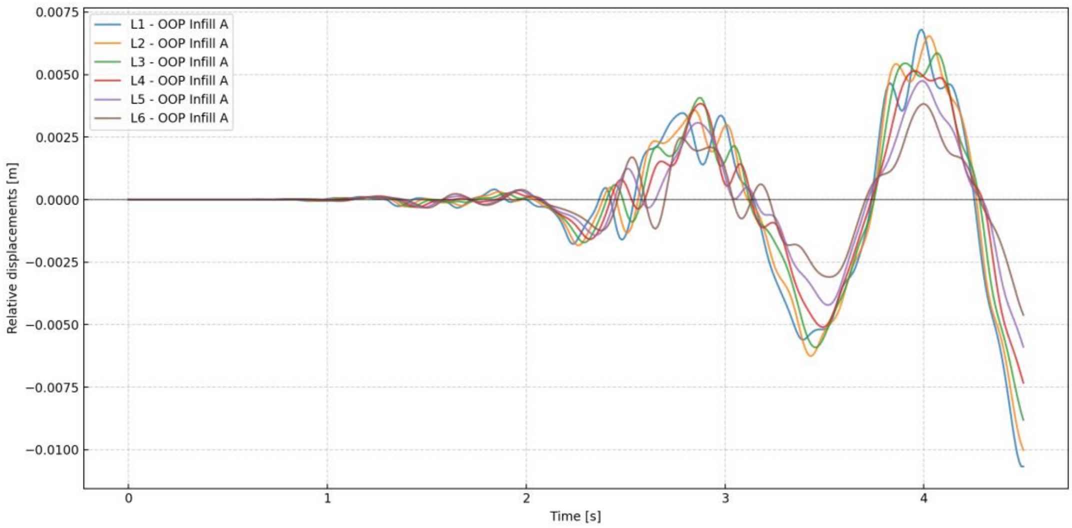

Figure 52 Dynamic analysis result for SBFI: Relative Out-of-Plane displacement time history results for all INFILL A middle point.

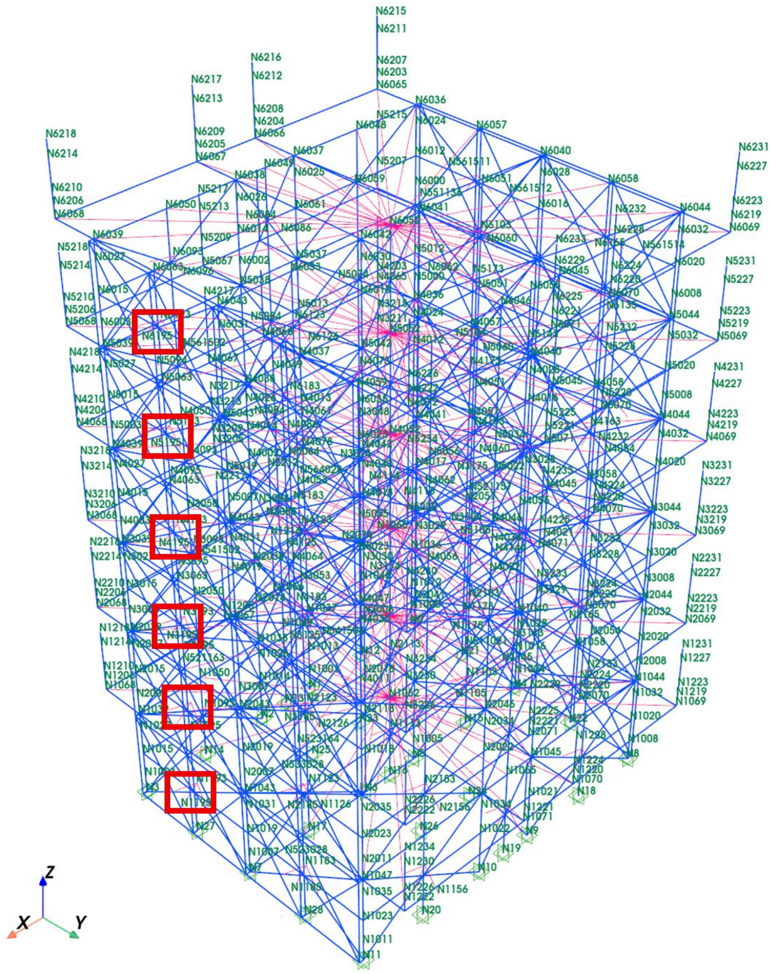

Figure 53 Spatial representation of the Strong Bare frame structure with infills enabled (SBFIR) and inside the red rectangle is denoted the infill nodes (INFILL A) that are monitored during the total seismic excitation (0.3g).

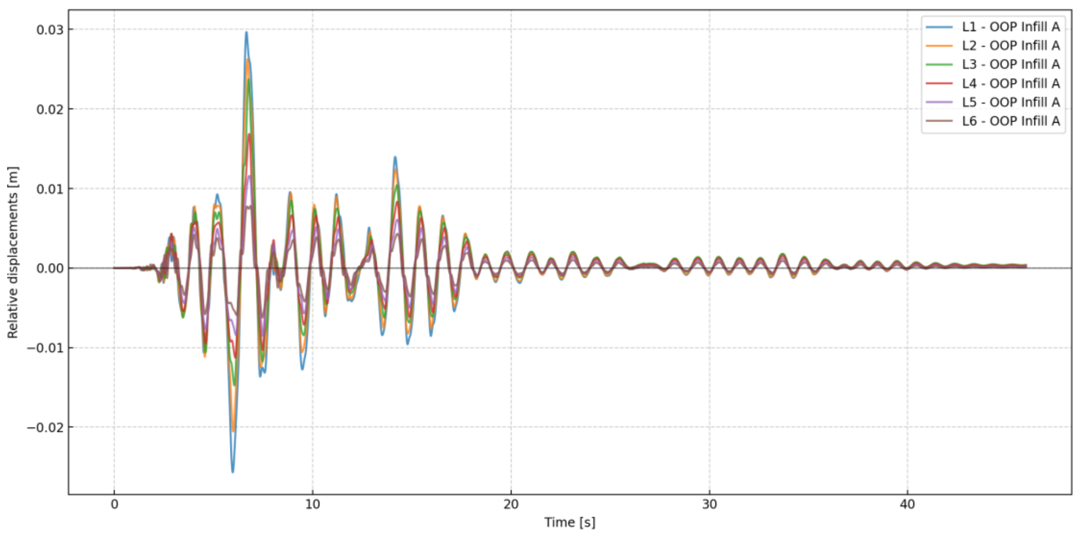

Figure 54 Dynamic analysis result for SBFIR: Relative displacement time history results for all INFILL A.

The out-of-plane (OOP) behavior of masonry infills is represented in Figure 47 through Figure 54. In the BFI and SBFI models, the infill nodes exhibit high-frequency oscillations with relative displacements reaching 1.5cm for the BFI with 3 sequential earthquakes, 1cm for the SBFI (but the analysis is terminated as the in-plane capacity of the infills is reached) and 3cm for the SBFIR. When compared to the retrofitted BFIR (Figure 50) and the SBFIR model (Figure 54), the following observations are evident:

- BFIR: Despite the increase in structural mass, which primarily affects the out-of-plane response, the infill response remains within initial ranges, preventing out-of-plane (OOP) collision with the Living Walls or OOP collapse (for repetitive near-field earthquakes) due to small displacements of approximately 1.5 cm.
- SBFIR: Despite the quadruple thickness and proportional mass increase, the maximum out-of-plane displacement is only doubled to 3 cm. This suggests that the chosen retrofitting-strengthening strategy (FRPU + PUFJ) provides sufficient out-of-plane constraint, significantly reducing the risk of infill collapse during a near-field severe seismic event.

9 INTEGRATED APPLICATIONS WITH THE HYBRID PLATFORM

This chapter presents the real-time integration of the structural monitoring system capabilities, using the example building examined in the previous chapters. This is done with the perspective that scaled or full-scale specimens could exist on a given shake table advanced equipment. The initialization of the hybrid platform begins with the creation of the model, which is described in detail in the GitHub codebase (Vanian & Rousakis, 2025). Figure 55 shows the results from the BFIR or SBFIR models; while their linear external geometry is the same, their cross-sections differ.

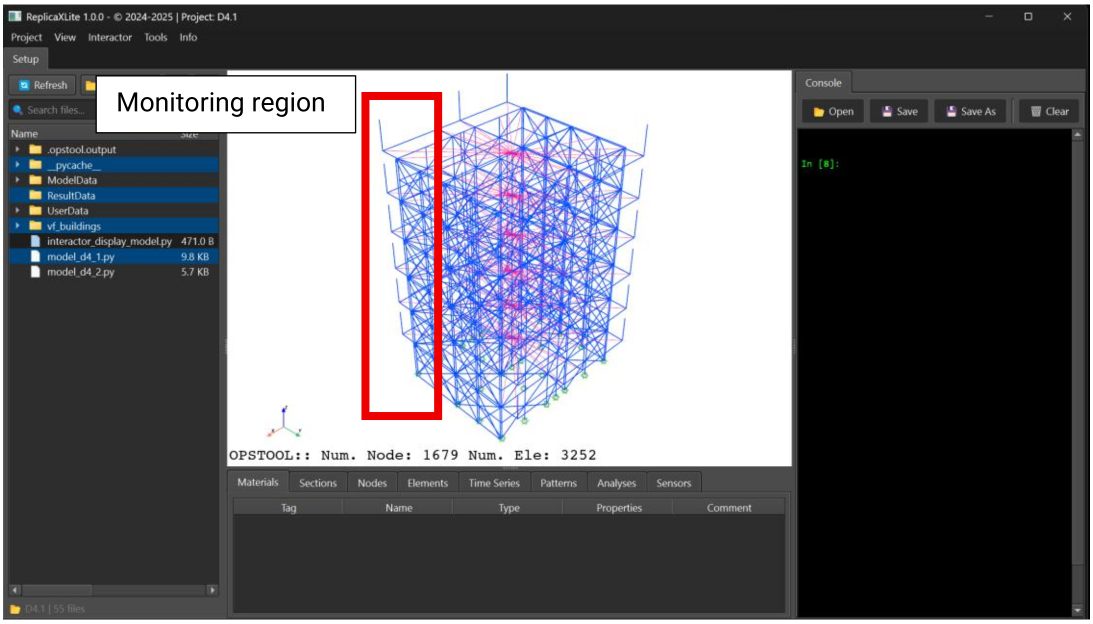

Figure 55 Hybrid platform stage of created model BFIR and SBFIR.

For demonstration purposes, only the real time monitoring of the left side of the building is presented, as denoted by the red rectangle in Figure 55. The same process is followed for any further points of interest. Accelerometer sensors are placed at the end of the vertical forest planters, in the mid-region of the vertical living wall, and on the infills in the out-of-plane direction. Finally, the presence of strain gauge measurements inside the reinforced concrete cross-sections, glued on steel rebars, with PZT sensors located nearby, is assumed.

These sensors are introduced into the model via the Sensors tab of the FEM table, as shown in Figure 56, by using the Ctrl++ shortcut and entering the necessary information. Under the 'Group' column, we use 'A' as a shortcut for accelerations. The sensor type is selected in the 'Type' column. Then, in the 'Sensor' cell, clicking the Table icon allows for the entry of the sensor name and its spatial location. Once the data is entered, the 'Close' button is clicked. In the 'Display' cell, select the 'True' option and provide the path for the sensor configuration file (e.g., the 'A.json' file) located inside the Sensor folder. Finally, click the 'Add' button and, if necessary, the 'Update' button to save any changes.

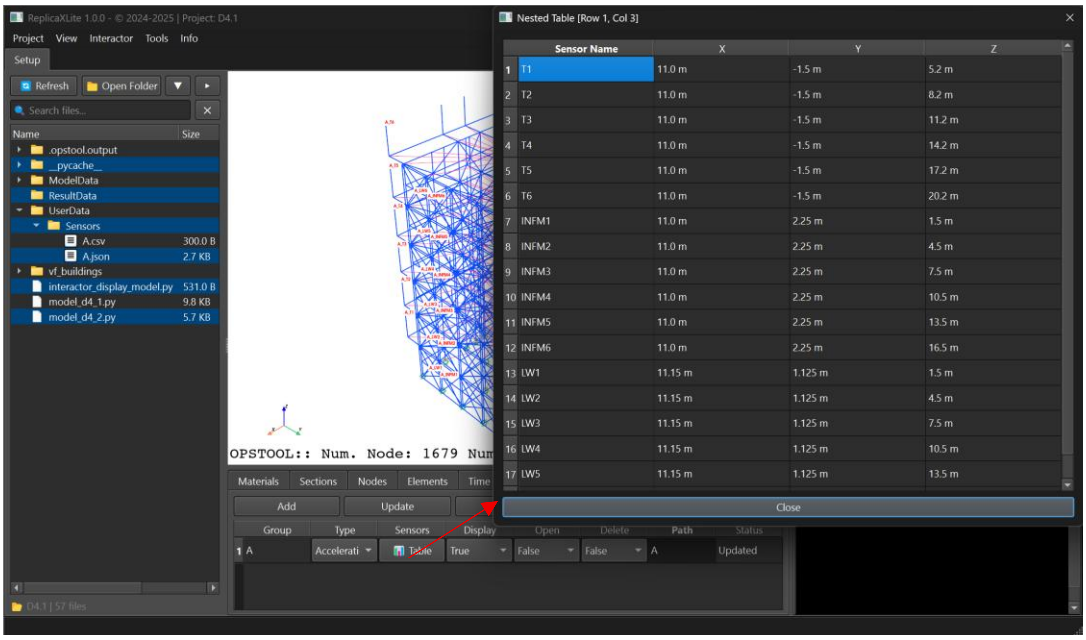

Figure 56 Hybrid platform stage of introducing new acceleration sensors.

Once the status is 'Updated' and the sensors are properly configured, setting the 'Open' cell to 'True' launches the Sensor GUI. This interface allows the data to be monitored, edited, and sent to the appropriate repository for further usage or archiving. All the information is provided in the documentation (Vanian & Rousakis, 2025).

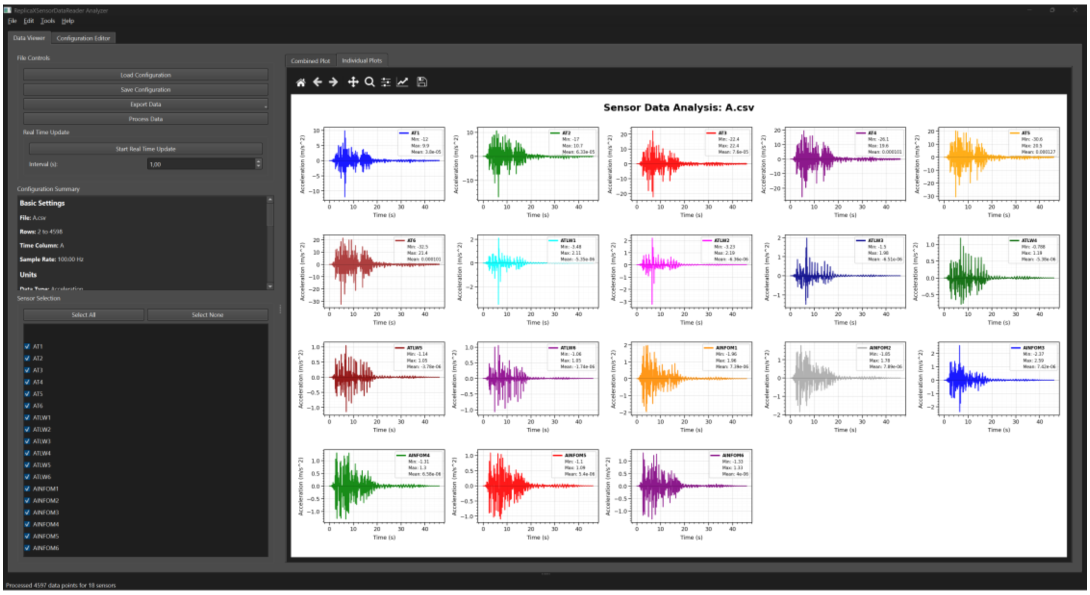

Figure 57 Hybrid platform stage of sensor live update and monitoring interface after clicking the process button.

The Graphical User Interface (GUI) is tightly connected with the Sensor API in a step-by-step format. This means that every time a significant change is made, the sensor information should be saved and reopened. This ensures that the data processing timeline is fully monitored. There is an option button for 'Real-Time' updates with a configurable interval, enabling the user to watch the introduction of data into the existing file in real time.

Accelerometer data can provide the necessary information to calculate displacement and, with proper processing, strain. This allows for a comparison between the calculated data and the PZT sensor information to determine if damage has accumulated in the structure. PZT data is introduced into the hybrid platform in a similar way to the acceleration information.

After processing the necessary information and determining the critical curves based on the section coordinate system, data for steel strain and stress over time can be derived (if not already recorded during database saving). This information can then be sent to other machines (experimental-pistons or analytical tools) to conduct detailed tests for the verification process (in example on steel rebars etc.). The example diagram of the information flow among the different equipment is denoted in Figure 58.

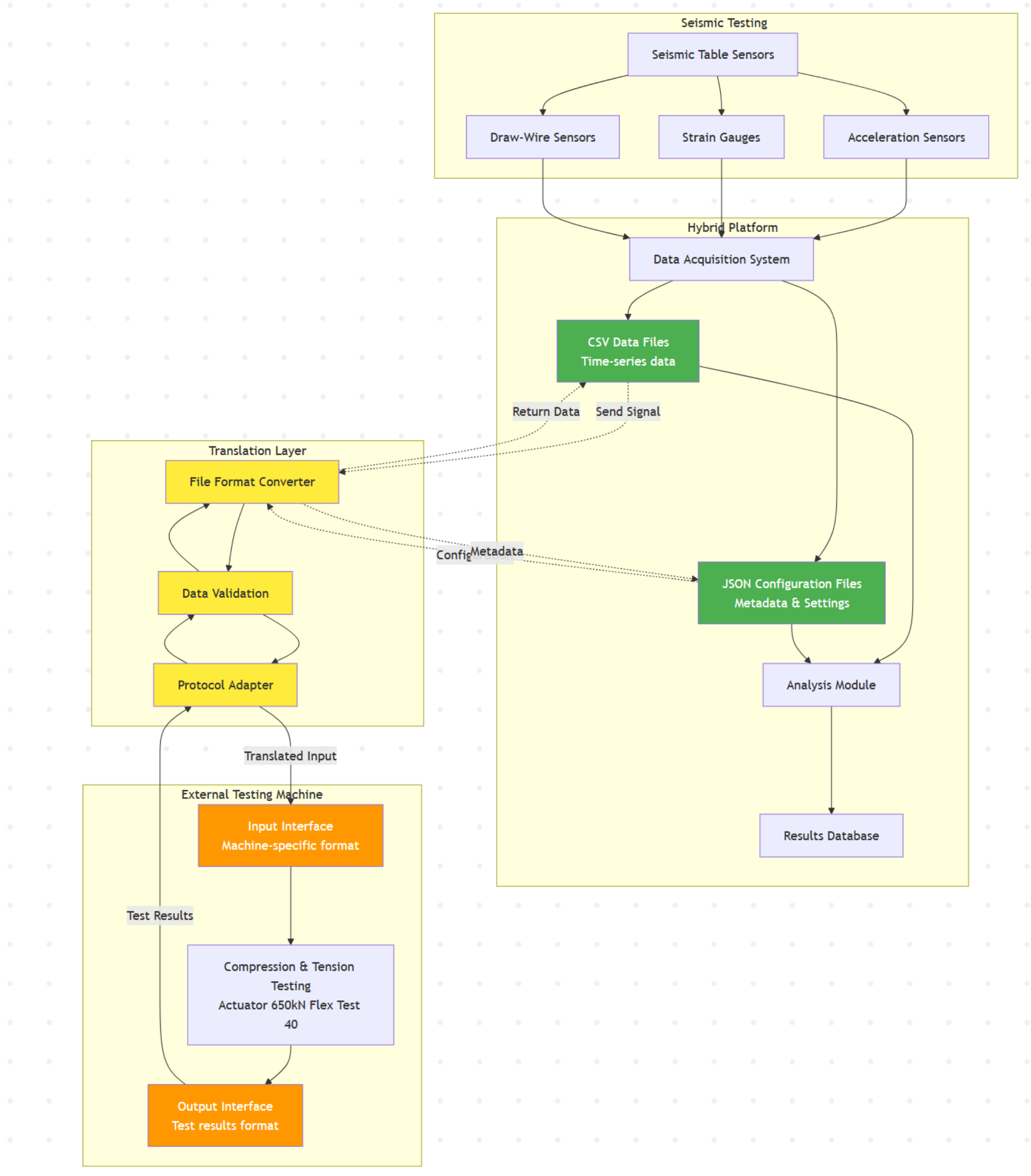

Figure 58 Hybrid platform interaction diagram.

10 CONCLUSION

The analysis demonstrated that the inclusion of "pilotis" (BFIP) creates a critical seismic vulnerability, evidenced by a longer fundamental period (0.979s) and a "soft-story" mechanism that causes damage concentration at the ground level, leading to a peak base shear of only ~1300 kN. In contrast, the "strong" infilled models (SBFI) exhibited the highest initial stiffness with respect to the increased mass, leading to lower fundamental period (T1=0.765s). The proposed retrofitting-strengthening strategy—employing 35mm seismic joints (PUFJ), confinement basalt ropes, and a Fiber Reinforced grid of Polyurethane matrix (FRPU)—successfully compensated for the added infrastructure and mass of the greenery renovations. In pushover analyses, the retrofitted BFIR model maintained its capacity up to ~0.28m top building displacement without significant degradation, compared to the standard BFI which terminated at ~0.11m.

Dynamic simulations further confirmed that the retrofitted SBFIR configuration could withstand a severe near-field Kobe earthquake scaled to 40% (0.3g PGA). While the existing non-retrofitted building (SBFI) reached multiple infill failures for the strong brick infills (0.5% drift) within the first 4 seconds, the retrofitted version sustained the full duration of the excitation record, accommodating drifts up to 2.5%. The study also proved the safety of the green components; the 2.2m tall trees experienced a maximum relative displacement of 0.10m during 0.3g near-field excitation. This represents only 6.7% of the 1.5m balcony clearance, effectively eliminating the risk of pounding or collision with the building facade.

Finally, the integration of the ReplicaXLite hybrid platform proved essential for real-time health monitoring. Provided the potential for open and customizable processing data from accelerometers, strain gauges (or even PZT, etc) sensors, the system creates a functional "digital twin" that validates the numerical models as depicted in deliverable 3.2 (Rousakis et al., 2025). The results conclude that combining high-strength infills with innovative retrofitting creates a high-base shear capacity system (~3000 kN base shear) with adequate top displacement ductility, ensuring that Vertical Forest renovations are not only architecturally viable but also seismically resilient in high-risk areas.

REFERENCES

Di Trapani, F., Shing, P. B., & Cavaleri, L. (2018). Macroelement Model for In-Plane and Out-of-Plane Responses of Masonry Infills in Frame Structures. *Journal of Structural Engineering*, *144*(2), 04017198. https://doi.org/10.1061/(ASCE)ST.1943-541X.0001926

Guo, J., Ye, A., Wang, X., & Guan, Z. (2023). OpenSeesPyView: Python programming-based visualization and post-processing tool for OpenSeesPy. *SoftwareX*, *21*, 101278. https://doi.org/10.1016/j.softx.2022.101278

Nafeh, A. M. B., & O'Reilly, G. J. (2022). Unbiased simplified seismic fragility estimation of non-ductile infilled RC structures. *Soil Dynamics and Earthquake Engineering*, *157*, 107253. https://doi.org/10.1016/j.soildyn.2022.107253

Papanikolaou, V. K., Kartalis-Kaounis, T., Protopapadakis, E., & Papadopoulos, T. (2017). GiD+OpenSees Interface: An Integrated Finite Element Analysis Platform. *Lab of R/C and Masonry Structures, Aristotle University of Thessaloniki*.

Pradhan, B., & Cavaleri, L. (2020). IP-OOP interaction in URM infilled frame structures: A new macro-modelling proposal. *Engineering Structures*, *224*, 111211. https://doi.org/10.1016/j.engstruct.2020.111211

Rahman, M. M., Nahar, T. T., & Kim, D. (2021). FeView: Finite element model (FEM) visualization and post-processing tool for OpenSees. *SoftwareX*, *15*, 100751. https://doi.org/10.1016/j.softx.2021.100751

Rousakis, T., Ilki, A., Kwiecien, A., Viskovic, A., Gams, M., Triller, P., Ghiassi, B., Benedetti, A., Rakicevic, Z., Colla, C., Halici, O. F., Zając, B., Hojdys, Ł., Krajewski, P., Rizzo, F., Vanian, V., Sapalidis, A., Papadouli, E., & Bogdanovic, A. (2020). Deformable Polyurethane Joints and Fibre Grids for Resilient Seismic Performance of Reinforced Concrete Frames with Orthoblock Brick Infills. *Polymers*, *12*(12), 2869. https://doi.org/10.3390/polym12122869

Rousakis, T., Vanian, V., Fanaradelli, T., Voutetaki, M., Zapris, A., & Theodoridou, I. (2025). *Investigation of the effects of renovations on VF structure: Greenergy-Resilient Vertical Forest Renovation of Reinforced Concrete Structures in Seismic Prone Areas (H.F.R.I. Project Number 015376)* [Deliverable D3.2]. Democritus University of Thrace, Xanthi.

Rousakis, T., Vanian, V., Lappa, M., Zapris, A. G., Xynopoulos, I. P., Voutetaki, M. E., Kellis, S., Sapidis, G. M., Naoum, M. C., Papadopoulos, N. A., Kytinou, V. K., Karabini, M., Thomoglou, A., & Chalioris, C. E. (2025). Assessment of Seismic Performance and Structural Health Monitoring of a Retrofitted Reinforced Concrete Structure with Polyurethane-Based Interventions and Vertical Greenery Systems. *Polymers*, *17*(23), 3104. https://doi.org/10.3390/polym17233104

Rousakis, T., Voutetaki, M., Vanian, V., Fanaradelli, T., & Zapris, A. (2024). *Literature review on VF buildings' modeling for combined renovation covering structural, energy, forestry and habitant comfort aspects. Greenergy-Resilient Vertical Forest Renovation of Reinforced Concrete Structures in Seismic Prone Areas (H.F.R.I. Project Number 015376). Deliverable D3.1*. Democritus University of Thrace, Xanthi.

Vanian, V., Fanaradelli, T., & Rousakis, T. (2025). A Comprehensive Review of Vertical Forest Buildings: Integrating Structural, Energy, Forestry, and Occupant Comfort Aspects in Renovation Modeling. *Fibers*, *13*(8), 101. https://doi.org/10.3390/fib13080101

Vanian, V., & Rousakis, T. (2025). ReplicaXLite: A finite element toolkit for creating, analyzing and monitoring 3D structural models. In *GitHub Repository* [Computer software]. GitHub. https://github.com/Vachan-Vanian/ReplicaXLite

Yan, Y., & Xie, Y. (2025). opstool: A Python library for OpenSeesPy analysis automation, streamlined pre- and post-processing, and enhanced data visualization. *SoftwareX*, *30*, 102126. https://doi.org/10.1016/j.softx.2025.102126